Breakthrough Behavior of H_2S Removal with an Iron Oxide Based CG-4 Adsorbent in a Fixed-Bed Reactor

A Thesis Submitted to the College of Graduate Studies and Research

in Partial Fulfillment of the Requirements

for the Degree of Master of Science

Department of Chemical Engineering

University of Saskatchewan

Saskatoon, SK

By

De Ming Wang

Permission to use

In presenting this thesis in partial fulfillment of the requirements for a Postgraduate degree from the University of Saskatchewan, I agree that the Libraries of this University may make it freely available for inspection. I further agree that permission for copying of this thesis in any manner, in whole or in part, for scholarly purposes may be granted by the professor or professors who supervised my thesis work or, in their absence, by the Head of the Department or the Dean of the College in which my thesis work was done. It is understood that any copying or publication or use of this thesis or parts thereof for financial gain shall not be allowed without my written permission. It is also understood that due recognition shall be given to me and to the University of Saskatchewan in any scholarly use which may be made of any material in my thesis.

Requests for permission to copy or to make other use of material in this thesis in whole or part should be addressed to:

Head of the Department of Chemical Engineering

University of Saskatchewan

Saskatoon, Saskatchewan, S7N 5A9

Abstract

Hydrogen sulfide (H_2S) is an environmentally hazardous, corrosive, and toxic gas, mostly generated in gas and oil industry. For small-scale natural gas processing sites (less than 10 tonne S/day), the use of regenerable iron oxide adsorbent to adsorb H_2S from natural gas is still an economical and effective method.

The objective of this research project was to understand the performance of an iron oxide adsorbent, recently emerging in the Canadian market, in removing H_2S from gas streams. To accomplish this, the breakthrough behaviors of H_2S adsorption in a fixed-bed reactor under elevated pressures were studied. The effects of variations in superficial velocity from 0.09 m/s to 0.26 m/s, operating pressure from 4 to 50 atm absolute, and the height of the fixed-bed from 11.7 cm to 24.5 cm on breakthrough curves and sulfur loading were investigated. In all the experiments, the H_2S concentration profiles of the exiting gas from the reactor were measured until the bed was saturated.

It was found that the shape of the breakthrough curves depend on the superficial velocity and the inlet H_2S concentration in gas streams. Under both higher superficial velocity and higher inlet H_2S concentration, the shape of the breakthrough curve becomes steeper. The sulfur loading of the adsorbent depends on the superficial velocity, the inlet H_2S concentration in gas streams, and the bed height. The sulfur loading decreases as the superficial velocity and the inlet H_2S concentration increase, but increases as the bed height increases. The change of

operating pressure does not have a significant effect on the shape of the breakthrough curve or sulfur loading of the adsorbent. The investigation was also extended using the regenerated adsorbents. A mathematical formula was developed to describe the breakthrough curves.

Acknowledgements

There are many people I would like to thank for their support, encouragement, and comments over the duration of this project. First, my supervisors, Dr. Hui Wang and Dr. Karl T. Chuang, deserve a great deal of credit for my academic formation. I would like to gratefully acknowledge their support and input. I would like to thank Dr. R. Evitts and Dr. A. Phoenix for their thoughtful feedback. Their questions and suggestions greatly improved the final product. Especially I would like to thank Dr. A. Phoenix for his revision and important suggestions for last version of my thesis.

I would like to thank Prof. Hanxian Guo of Taiyuan University of Technology for the beneficial discussions with him.

Richard Blondin, Ted Wallentity, and Dragan Cekic, of the department of Chemical Engineering were always there offering solid support.

My fellow graduate students were the most important ingredient during this period. A special thanks to Jianguo Zhang, Zhiguo Wang, and Robert St. Pierre for taking time to give a lot of advice.

Last but not least, to my wife and my daughter who were there throughout it all. Thank you for always being by my side, encouraging me, and comforting me. Your unwavering belief that I can do anything is truly overwhelming but incredibly empowering.

Dedication

To my parents, wife, and daughter

Table of Contents

List of Tables

List of Figures

Nomenclature

A	gaseous reactant (H_2S)
B	solid reactant (adsorbents)
C	dimensionless concentration
C_A	gaseous reactant concentration (H_2S) , mol/m^3
$C_{A,in}$	gaseous reactant concentration in feed stream, mol/m^3
C_B	solid reactant concentration (adsorbents) , mol/m^3
C_{B0}	solid reactant concentration (adsorbents) at initial state, mol/m^3
C_{eq}	equilibrium concentration, mol/m^3
D	molecular diffusion coefficient, m^2/s; or inside diameter , m
D_e	effective diffusion coefficient, m^2/s
D_g	gas diffusion coefficient, m^2/s
D_k	Knudsen diffusion coefficient, m^2/s
$F(X)$	dependency of conversion rate on solid reaction concentration
k	rate constant, or Boltzmann's constant
K	dimensionless constant
L_{E0}	total length of pore, m
L	characteristic length for adsorbent pellets, m
L_0	bed length of fixed-bed, m

L_t	length of the transition zone, m
MW_S	molecular weight of sulfur
MW_{H_2S}	molecular weight of hydrogen sulfide
n	apparent reaction order
P_c	critical pressure, bar
Pe	Peclet number
R	pellet radius, m
R'	defined by Eq. 2.51
r_g	initial grain radius
S_{E0}	surface area cylindrical pore, m^2
S_0	specific surface area of adsorbent, m^2/g
t	reaction time, s
T_c	critical temperature, K
t_b	breakthrough time, s
t_c	saturation time, s
t_s	stoichiometric time, s
u_t	moving velocity of the transition zone, m/s
u_g	superficial velocity of the gas into the reactor, m/s
V_{H_2S}	volumetric rate of feed stream, m^3/s
W_{fb}	adsorbent loading in the fixed-bed reactor, g
X	fractional conversion of solid reactant
z	dimensionless variable defined in Eq. 2.42
Z	axial coordinate in the bed, m

Greek letters

ε	characteristic energy
ε_0	initial porosity of the fresh adsorbent
ε_p	porosity of the adsorbent particle
ε_{fb}	porosity of the fixed bed (bed void fraction)
ρ	density (mol/m^3)
σ	characteristic length (Å)
τ	time defined by Eq. 3.17 (s)
	or tortuosity factor for the sorbent particle.
ψ	structural parameter defined by 2.21
ψ_s	sphericity of a particle

Chapter 1

Introduction

1.1 Overview

Hydrogen sulfide (H_2S) is present in natural gas and biomass gas. It is also formed in oil production and coal gasification. It is a significant health risk in addition to causing air pollution, acid rain, and corrosion.

A significant portion of natural gas production contains an acid gas component such as H_2S. Natural gas is considered "sour" if H_2S is present in amounts greater than 5.7 milligrams per normal cubic meter. The H_2S must be removed to meet the pipeline and sales specifications (less than 4 parts per million, or ppm, in volume) (Clean Air Act, 1989).

A number of processes are available to remove H_2S from gas streams. Prior to the early 1990s sulfur recovery and acid gas flaring were the most economic methods of dealing with the acid gas streams (Bachu and Gunter, 2005). Acid gas less than 10 tonnes sulfur per day is flared because this scale is too small to run sulfur recovery process economically. The Claus process-tail gas treating is suitable for gases with a H_2S concentration of 20 % v/v on a large scale of more than 25 tonnes sulfur per day (Speight, 1990) (Wang *et al*., 2008). As a result of public concern, human and animal health, and environmental degradation, the use of flaring H_2S-containing acid gas is restricted. On the other hand, due to a weak sulfur market sulfur recovery processes have recently become uneconomic (Wang *et al*., 2008). Therefore, the technologies of long-term storage of sulfur or

hydrogen sulfide are attracting research attention in Canada. Injecting the high–pressure acid gas in depleted oil wells for long term storage is recently pursued by gas companies in order to eliminate flaring acid gas. This method poses risks to public safety due to the potential of toxic gas leakage. Long-term storage methods of elemental sulfur such as burying it in remote areas was investigated (Davis *et al*., 2004). However, neither injecting acid gas nor burying elemental sulfur from sulfur recovery is cost effective (Wang *et al*., 2008).

For small-scale natural gas productions of less than 10 tonnes of sulfur per day, H_2S adsorption by iron oxide medium is an effective and economical method of removing H_2S from gas streams. Iron oxide adsorbent works by reacting H_2S and turning ferric oxide into ferric sulfide. The ferric sulfide can be converted back into ferric oxide as well as elemental sulfur when exposed to oxygen or air.

A ferric oxide based adsorbent, CG-4 provided by CLEAN Catalysis and Purification Technologies Development Company in Shanxi Province, China, is used in some small gas plants in Canada. Its one-time sulfur loading can be as high as 15 % w/w (1 kg of the adsorbent can take in 0.15 kg elemental sulfur before breakthrough of H_2S) (Wang *et al*., 2008). Wang *et al.* also proposed a safer acid gas disposal method by adsorbing H_2S from natural gas with CG-4 adsorbent. The spent adsorbent slurry, which is produced by removing the adsorbent from the adsorbing towers by high-pressure water, can then be injected into depleted oil and gas wells. The regeneration of CG-4 adsorbent using ammonia leaching has been studied (Wang *et al*., 2008). The regeneration allows the adsorbent to be used for several adsorption-regeneration cycles before being

replaced. By increasing the lifetime of the adsorbent, the utilization efficiency of the adsorbent is improved.

Using the CG-4 sorbent to remove H_2S from natural gas is still new to the Canadian gas industry. Wang *et al*. (2008) investigated the sulfur loading of this adsorbent and regeneration by ammonia leaching. There is a lack of kinetics data of the chemical adsorption process in a fixed-bed reactor under the operating conditions of gas processing plants.

The breakthrough behaviors in a fixed-bed reactor represent the global reaction kinetics including gas flow, mass transfer, and intrinsic kinetics. They can be obtained by measuring the concentration of H_2S at the outlet end of the fixed-bed. The size of a fixed-bed is determined by different factors such as the utilization efficiency of the adsorbent, the time period of operation, the operating conditions, and the pressure drop in the bed.

1.2 Objectives of this research

The overall objective of this research is to understand the adsorption process of the CG-4 iron oxide adsorbent in a fixed-bed. This goal will be achieved by investigating the sulfur loading and H_2S breakthrough curves of CG-4 iron oxide adsorbent under different operating conditions: pressures of 4-50 atm absolute, superficial velocities from 0.09 to 0.26 m/s, and H_2S concentrations between 0.50 and 6.01% v/v. A second objective of this project is to establish a simple mathematical model for this process.

1.3 Organizations of the thesis

This thesis is organized in five chapters. Chapter 1, Introduction, introduces the background, the latest developments in H_2S removal processes, and the reason and objectives of this project. Chapter 2, Background and Literature Review, reviews characteristics and emissions of H_2S, emission controlling technologies, and the theories and current research related to H_2S adsorption technologies. Chapter 3, Experimental Methods, introduces the experimental setup and methods for analyzing the composition of a gas mixture in order to determine the breakthrough curves. Chapter 4, Results and Discussions, focuses on discussing the effects of changing the operating conditions on the breakthrough curves and the mathematical model proposed to represent the breakthrough curves. Finally, Chapter 5, Conclusions and Recommendations, summarizes conclusions drawn from the discussion and presents suggestions and directions for further development.

Chapter 2

Background and Literature Review

Sulfur removal from industrial gas streams is practiced in natural gas, refining, and coal gasification industries. The gas streams produced during petroleum refining contain H_2S adversely affecting the use of gas for other purposes, for instance, as a fuel or as a petrochemical feedstock. Some degree of cleaning is required due to health concern associated with H_2S or due to the potential of H_2S to poison catalysts. Under the reducing environment of coal gasification, the sulfur in coal is released as H_2S in the gas products, and a gas treating to remove the H_2S is required. Sour natural gas containing H_2S is subjected to processing to reduce H_2S concentration to less than 4 ppm (Clean Air Act, 1989). Sulfur removal has formed an important section in these industries and there are a number of processes for removal of sulfur from gas streams. In deciding which process to use, several factors must be considered including the required extent of H_2S removal; the gas composition, temperature, volume and pressure; and the impact of sulfur recovery on the process economics and/or the environment. The Claus process is a technology that is able to remove H_2S from a gas stream and recover sulfur in elemental form. However, the Claus process is only economical for large scale production due to its large capital investment and complex procedures (Wang *et al*., 2008). For small scale gas productions of less than 10 tonnes of sulfur per day, H_2S adsorption by an adsorbent is a good choice (Wang *et al*., 2008). In this chapter the properties of H_2S are briefly covered,

followed by a review of H_2S removal technologies and processes with a focus on a small scale gas processing, dry adsorption by adsorbents, and related gas-solid reaction theories and research.

2.1 Hydrogen sulfide

2.1.1 Properties

Hydrogen sulfide is a colorless, highly flammable, and extremely toxic gas with a characteristic odor of rotten eggs. The odor threshold for humans is as low as 1 ppm. It is slightly soluble in water (0.4 % w/w at 20 °C) and the pH value of a H_2S-saturated aqueous solution is 4.5. Five minutes of exposure to 1,000 ppm H_2S in air can be fatal to humans (Patnaik, 1999). If exposed to H_2S, symptoms can include headache, nausea, nervousness, cough, eye irritation, and insomnia. High doses can cause unconsciousness, respiratory paralysis, and death. For detailed information on hazardous properties see the MSDS of H_2S provided by Praxair (Appendix G). H_2S in solution is corrosive and therefore damages the equipment which it contacts. It is poisonous to many industrial catalysts as well.

2.1.2 Analysis of H_2S

H_2S can be detected when the gas turns a paper soaked in a lead acetate solution black. Many infrared sensors are commercially available for *in-situ* measurements of H_2S. It may be monitored semi quantitatively by a Draeger tube H_2S detector (Xue, 2003). It is most often analyzed by GC analysis with either a TCD (thermal conductivity detector), a FPD (flame photometric detector), or a sulfur chemiluminescence detector.

2.1.3 Occurrence of H_2S

The typical concentration of H_2S in natural gas is within 0-5 % v/v. The H_2S concentration in the gases formed in oil production is between 6 % v/v and 8 % v/v. There is less than 1 % v/v sulfur impurity in biomass gas. Concentrated H_2S gas streams can be generated in some industrial processes such as metallurgical processes (Speight, 1990).

2.2 Technologies for removal of H_2S from gaseous streams

The focus in this study is on the gaseous streams in natural gas processing with a H_2S content of less than 8 % v/v. The available technologies for H_2S scavenging from gas streams of this H_2S concentration fall into two categories: Dry sorption processes and Liquid processes.

2.2.1 Dry sorption processes

The dry H_2S removal techniques discussed involve the use of dry adsorbents in towers that allow gas to flow upwards or downwards through the media. Since all of the dry-sorption media will eventually become saturated with contaminant and become inactive, it is common to have two vessels operated in parallel so one vessel can remain in service while the other is offline for media change-over (so called “swing operation” or lead/lag configuration).

Dry sorption processes can be categorized into two sub groups: physical sorption and chemical sorption.

Chemical sorption processes are governed by the reaction of an adsorbent with H_2S to form a compound.

Many metal oxides of metals such as Fe, Mo, Zn, Ca, Ba, Sr, Cu, W, and Co can be used as suitable adsorbents for the removal of H_2S (Xue, 2003). The primary oxides of metals used for chemical sorption processes are iron oxide, zinc oxide and calcium oxide.

As one of the oldest sulfur removal methods, the iron oxide process was implemented during the 19th Century (Crynes, 1977). Iron oxide adsorbents remove sulfur by forming insoluble iron sulfides and the spent adsorbents can be regenerated by oxidizing the iron sulfides with air. But eventually the media becomes clogged with elemental sulfur and must be replaced after several recycles.

The reaction of sulfur removal using iron oxide adsorption (Crynes, 1977; Kouichi Miura et al., 1992) is:

$$H_2S(g) + \frac{1}{3}Fe_2O_3(s) \rightarrow \frac{1}{3}Fe_2S_3(s) + H_2O(l) \quad (2.1)$$

$$\Delta H = -22 \text{ kJ} \quad \text{(at 25 °C and 1 atm)} \quad (2.2)$$

This reaction is best carried out at room temperature, otherwise the iron oxide complex is dehydrated, greatly reducing the reaction rates or decomposing Fe_2S_3 to FeS_2 and Fe_8S_9 which are difficult to regenerate.

The regeneration reaction of spent adsorbents is:

$$\frac{1}{3}Fe_2S_3(s) + \frac{1}{2}O_2(g) \rightarrow \frac{1}{3}Fe_2O_3(s) + S(s) \quad (2.3)$$

$$\Delta H = -198 \text{ kJ} \quad \text{(at 25° C and 1 atm)} \quad (2.4)$$

Because of the highly exothermic nature of the regeneration reaction (2.3), the spent adsorbents may be pyrophoric when exposed to air and thus the attention should be focused on the safety during change-out.

The active iron oxide products are sold under several trademarks utilizing different support media, such as Iron Sponge, SulfaTreat, Sulfur-Rite, Media-G2, and CG-4. Their detailed information is listed in the Table 2.1.

Zinc and calcium oxides have been studied and are also widely used to remove H_2S through the following reactions:

$$ZnO + H_2S \rightarrow ZnS + H_2O \quad (2.5)$$

$$CaO + H_2S \rightarrow CaS + H_2O \quad (2.6)$$

Calcium oxide is the better choice for H_2S adsorption at elevated temperatures (250-500 °C) and ZnO appears to be good at temperatures lower than 100 °C (Xue, 2003).

In addition, alkaline substances can be used to react with acid gases, like H_2S and SO_2, in neutralization reactions. Usually liquid processes are used, but fixed-beds of alkaline granular solid can also be used with an upward or downward gas flow (Kohl, 1997).

A different approach to H_2S removal is to rely on the physical adsorption of H_2S onto a solid surface rather than chemical reaction. Media developed with high surface areas and large pore volumes eventually become saturated at low temperatures and high pressures, and must be regenerated at high temperature and low pressures. During regeneration, a H_2S rich gas is released and must be subjected to another process for sulfur recovery.

Table 2.1 Comparison of iron oxide –based H_2S removal processes

Packing	operating conditions	Regenerable	Media Cost ($/kg H_2S removed)	Notes	Suppliers
Iron Sponge	20-23 ºC 60 sec residence time	2-3 times in batch mode only	0.35-1.55	Labor intensive	Connelly GPM, Physichem, Varec Vapor control
Sulfa Treat	20~ 23 ºC 60 sec residence time	No	4.85-5.00	Non-pyrophoric and easier handling	Sulfatreat
Sulfur Rite	20~ 23 ºC 60 sec residence time	No	7.95-8.50	Prepackaged modules; forms iron pyrite	US Filter/ Merichem
Media-G2	20~ 23 ºC 60 sec residence time	15 times in batch mode only	2.90-3.00	Requires multiple regenerations to obtain estimated removal efficiency	ADI International
CG-4	20~ 23 ºC 60 sec residence time	2-3 times in batch mode only	3.50-4.00	High sulfur loading and easier handling	CLEAN Catalysis and Purification Technologies Development Company

Source: 1. www.bioway.net, Dec. 26, 2007. 2. for CG-4 from manufacturer

Molecular sieves (zeolites) are naturally occurring or synthetic silicates with very uniform pore sizes and high pore volumes making them ideal for adsorption. Polar compounds, such as water, H_2S, SO_2, and NH_3, are very strongly adsorbed. Granular activated carbon (GAC) is made by heating carbon–containing materials to drive off volatile components, forming a highly porous adsorptive surface. This method is preferable for removal of VOC (volatile organic compounds) from gas streams. If GAC is used to remove H_2S, coating it with alkaline or oxide solids enhances the sulfur capacity of the carbon due to chemical reaction.

2.2.2 Liquid H_2S processes

Liquid-based H_2S removal processes can reduce ground-space requirements, labor costs and increase the potential for elemental sulfur recovery. Gas-liquid contactors are used to increase contact surface area and maximize gas contact time (Wang, 2004).

2.2.2.1 Scrubbing and stripping process

Hydrogen sulfide is an acid when dissolved in water:

$$H_2S\,(g) \rightarrow H_2S\,(aq) \rightleftharpoons H^+ + HS^- \qquad (2.7)$$

If chemicals are added to the solution that can consume either H^+ or HS^- then more hydrogen sulfide can dissolve in the solution. The obvious choice is some alkali, a source of OH^-. Removing the H^+ on the right side of Eq. (2.7) drives the equilibrium to the right hand side, greatly increasing the amount of hydrogen sulfide absorbed.

In order to regenerate the solvent, the alkali should be a weak base that can easily release the acid gas on heating or pressure reduction. The most common choices of alkali for hydrogen sulfide removal are ethanol amines (monoethanolamine, diethanolamine, triethanolamine) and sodium or potassium salts of weak acids such as carbonic acid or phosphoric acid. Monoethanolamine reacts with H_2S to form an amine sulfide and hydrosulfide (Wang, 2004):

$$2HOCH_2CH_2NH_2 + H_2S \rightleftharpoons (HOCH_2CH_2NH_3)_2S \quad (2.8)$$

$$(HOCH_2CH_2NH_3)_2S + H_2S \rightleftharpoons 2HOCH_2CH_2NH_3HS \quad (2.9)$$

2.2.2.2 Biological method to remove hydrogen sulfide from a gas stream

Biological oxidation has been used for odor control in gas streams containing hydrogen sulfide. As an example, hydrogen sulfide is converted to sulfuric acid by the following reaction in aerobic conditions:

$$H_2S + 2O_2 \xrightarrow{\text{bacteria}} H_2SO_4 \quad (2.10)$$

The gas stream is first humidified and warmed as needed. Then it passes through a packed-bed biofilter where the H_2S is absorbed into a liquid film and oxidized by sulfating bacteria. Collected water is removed to a sanitary drain. The efficiency of hydrogen sulfide removal can reach 99% or greater with inlet concentrations of up to 1000 ppm (Sublette, 1987).

As another example, under anaerobic conditions the following reaction takes place in the presence of light and photoautotrophic bacteria (Sardesai, 2006):

$$2H_2S + CO_2 \xrightarrow[\text{bacteria}]{\text{light}} 2S + (CHO) + H_2O \quad (2.11)$$

During this process, carbon dioxide is fixed in the form of cell biomass and H_2S is oxidized to elemental sulfur in the presence of light. Photoautotrophic bacteria provide nearly 100% sulfide removal.

2.3 Modeling of non-catalytic gas-solid reactions

From a chemical principle point of view, the removal of H_2S by iron oxide adsorption is a typical non-catalytic, gas-solid reaction which takes place in a fixed-bed reactor. Therefore the following literature survey focuses on the following: (1) non-catalytic gas-solid reaction models; (2) H_2S removal by adsorption; and (3) breakthrough curve behavior.

2.3.1 Non-catalytic gas-solid reaction models

Non-catalytic gas-solid reactions represent an important category of heterogeneous reactions. A great number of models have been developed to describe the kinetics of gas-solid reactions. Some of them, such as the "unreacted shrinking core model" (Levenspiel, 1972), do not require specific knowledge of the internal structure of the reacting solid. Other models, such as the "grain model" (Szekely *et al.*, 1976), require the knowledge of physical parameters characterizing the internal structure of the solid i.e., the specific surface area or the average pore size. Some even include such considerations as pore-size distribution, change of porosity during the reaction, and pore plugging in the course of the reaction (Bhatia and Perlmutter, 1981; Froment and Bischoff, 1991). The models demand more extensive and precise information about the structure of the reacting solid.

2.3.1.1 Unreacted shrinking core reaction model

The unreacted shrinking core reaction model (Levenspiel, 1972) was developed for the situation when the diffusivity in the core of the pellet is so much lower than that in the reacted layer that virtually no gaseous reactant can reach the unreacted core, and a distinctive front of reaction exists as shown in Figure 2.1.

The model gives the time necessary to reach a given conversion of the solid:

$$t = \tau_{DP}[1-3(1-X)^{2/3}+2(1-X)]+\tau_{MT}[X]+\tau_{R,SC}[1-(1-X)^{1/3}] \tag{2.12}$$

in which τ_{DP}, τ_{MT}, $\tau_{R,SC}$ and X are defined as follows:

$$\tau_{DP} = \left(\frac{\rho_s}{6(C-C_{eq})}\right)\left(\frac{R^2}{D_e}\right) \tag{2.13}$$

$$\tau_{MT} = \left(\frac{\rho_s}{3(C-C_{eq})}\right)\left(\frac{R}{K_g}\right) \tag{2.14}$$

$$\tau_{R,SC} = \left(\frac{\rho_s}{C-C_{eq}}\right)\left(\frac{R}{K_s}\right) \tag{2.15}$$

$$X = 1-(R_C/R)^3 \tag{2.16}$$

where τ_{DP} is the characteristic time for diffusion through the pellet's product layer, τ_{MT} the characteristic time for external mass transfer from the bulk gas to the surface of the pellet (film diffusion), and $\tau_{R,SC}$ the characteristic time for chemical reaction at the interface between the unreacted core of the pellet and the reacted product layer, and X is the conversion of the pellet.

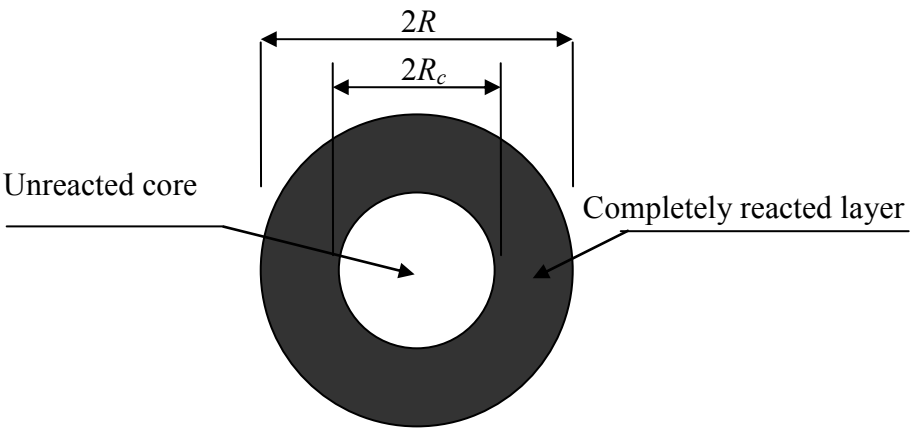

Figure 2.1 Schematic diagram for unreacted shrinking core model

2.3.1.2 Grain model

The grain model assumes that the solid structure consists of a matrix of very small grains, usually spherical in shape. The first grain model was established by Szekely and Evans (1976) who applied the grain model theory by assuming that the shrinking grains of solid reactant are surrounded by a dense layer of solid product with uniform thickness. Most early grain models assume that the overall grain size remains constant during the course of the reaction.

If the diffusivity of the gaseous reactants (or products) in the core of the reacting pellet is not significantly lower than that in the completely (or partially) reacted layer, then the gases have the potential to reach the center of the pellet even if only a thin outside layer of the pellet is reacted. This is shown in Figure 2.2. The dark parts of the grains represent the product layer. The relationship between reaction time and conversion is:

$$t = (\tau_{DP} + \tau_{DG})[1 - 3(1-X)^{2/3} + 2(1-X)] + \tau_{MT}[X] + \tau_{R}[1-(1-X)^{1/3}] \qquad (2.17)$$

with:

$$\tau_{DG} = \left(\frac{\rho_s}{6(1-\varepsilon_V)(C - C_{eq})} \right) \left(\frac{r_g^{\,2}}{D_g} \right) \qquad (2.18)$$

$$\tau_{R} = \left(\frac{\rho_s}{(1-\varepsilon_V)(C - C_{eq})} \right) \left(\frac{r_g}{K_S} \right) \qquad (2.19)$$

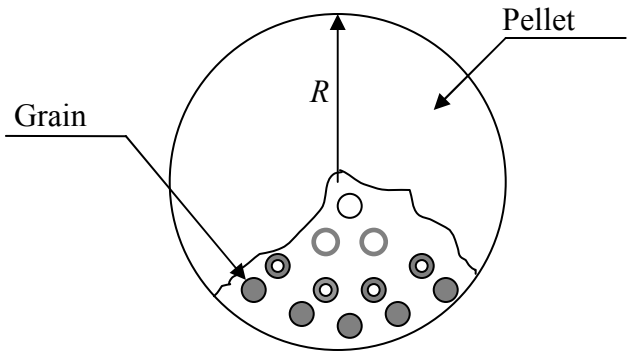

Figure 2.2 Schematic diagram for a grain model (dark parts of the grains represent the product layer)

where τ_{DG} is the characteristic time for diffusion through the grain and τ_R is the characteristic time for chemical reaction at the interface between the unreacted core and the reacted layer of the grain. τ_{DP} and τ_{MT} are defined the same as in the unreacted shrinking-core model using Eqs (2.13) and (2.14) respectively.

The local conversion at each time and position inside the particle is calculated with the following equations (for the grains, the kinetics are according to the shrinking core reaction model):

$$X(R,t) = 1 - (r / r_g)^3 \tag{2.20}$$

$$r_g = 3(1-\varepsilon) / (S_0 \rho\, MW) \tag{2.21}$$

where S_0 is the specific surface area (m^2/g) of solid; ρ is density (mol/m^3) of solid; and MW is the molecular weight (g/mol) of solid.

The mean conversion at each time in the whole particle is calculated by integrating the following equation:

$$X(t) = \left[\int_0^R 4\pi R^2 X(R,t)\, dR \right] / (\frac{4}{3}\pi R^3) \tag{2.22}$$

This grain model is based on the hypothesis of non-overlapping grains. The notion of overlapping was further pursued by Sotirchos and Yu (1988), who derived analytical expressions for the structural properties of porous media whose solid phase is represented by a population of randomly overlapping grains of uniform or distributed size. Recently, Efthimiadis and Sotirchos (1993) used an overlapping distribution grain model showing the importance of grain size in solid behavior.

2.3.1.3 Random pore model (RPM)

The original random pore model developed by Petersen (1957) treated the pore distribution as an idealized network of randomly intersecting cylindrical pores. A more refined random pore model for a distributed pore size system was presented by Bhatia and Perlmutter (1981a, b). Their model considers the reaction surface to be the result of the random overlapping of a set of cylindrical surfaces of size distribution $f(r)$. The total length of the system, L_{E0}, and the surface area, S_{E0}, are related to the structural parameter Ψ by means of the expression:

$$\psi = \frac{4\pi L_{E0}(1-\varepsilon_0)}{S_{E0}^{\ 2}}. \tag{2.23}$$

L_{E0} and S_{E0} can be measured by N_2 adsorption (BET) and the voidage, ε_0 can be measured by the mercury porosimetry.

A mass balance in a pore must be conducted to relate the concentration in the pores with that of the interface, assuming a linear gradient in the product layer. With this balance and the preceding equations Bhatia and Perlmutter (1980) determined an expression for calculating the local reaction rate:

$$\frac{dX}{dt} = \frac{CS_0 k(1-X_S)\sqrt{1-\psi\ln(1-X)}}{(1-\varepsilon_0)\rho_{molar}\left[1+\frac{\beta Z}{\psi}\sqrt{1-\psi\ln(1-X)}\right]} \tag{2.24}$$

$$\beta = 2k(1-\varepsilon_0)/DS_0. \tag{2.25}$$

Because this model does not consider progressive pore plugging, the structural parameter, Ψ, has a constant value.

The H_2S reaction with the iron oxide adsorbent is a specific case of a gas-solid reaction in which structural changes take place inside the adsorbent as the

reaction proceeds. Thus, the structural parameters in the above models change during the reaction period and can be calculated as follows:

The effective diffusivity is calculated as a function of the particle porosity and the tortuosity factor of the particle (Adanez *et al*., 1998) using Eq. (2.26).

$$D_e = D_g \varepsilon_p / \tau \,. \tag{2.26}$$

The effective diffusivity depends on the type of gas diffusion occurring in the pores: molecular, Knudsen, or a combination of both. Knudsen diffusion is generally restricted to pores smaller than 100 nm in diameter, and molecular diffusion is found in pores larger than 1000 nm in diameter (Welty, 2001). Because of the variation in the size of the pores during the reaction, the gas diffusivity was calculated as a combination of molecular and Knudsen diffusion:

$$D_g = [D^{-1} + D_k^{-1}]^{-1} \,. \tag{2.27}$$

The tortuosity was calculated using the equation of Wakao and Smith (1962) and later modified by Elias- Kohav *et al.* (1991) by introducing a parameter, *b*, to define different porous structures of the solids:

$$\tau = 1/(\varepsilon_p)^b \,. \tag{2.28}$$

For these materials, if an average pore diameter is assumed, a reasonable approximation for the effective diffusion coefficient in random pores (that is b=1) is (Ilaria Rosso, 2003)

$$D_e = D_g (\varepsilon_p)^2 \,. \tag{2.29}$$

The changes in porosity inside the particle with conversion are calculated using the Hartman and Coughlin (1976) expression as a function of the initial porosity, ε_0, and the expansion ratio, Z:

$$Z = \frac{\rho_{Fe_2O_3}}{\rho_{Fe_2S_3}} \tag{2.30}$$

$$\varepsilon_p = \varepsilon_0 - (Z-1)(1-\varepsilon_0)X\,. \tag{2.31}$$

then the density of the adsorbent solids are calculated by the following expression:

$$\rho_{molar} = \rho X / (1-\varepsilon_p)\,. \tag{2.32}$$

2.3.2 Solution of these models

Most of the models require computational solutions as analytical solutions can not be found for most of the rate forms used to describe these systems (Ramachandran, 1983). An extensive review of the computational aspects of these models can be found in the literature (Xu and Hoffmann, 1989; Patisson *et al*., 1998).

Gottifredi and Gonzo (1996, 2005) developed one of the most generalized solutions found for the isothermal, catalytic, steady-state case. Their solution allows for the determination of simple analytical predictions of the effectiveness factor and gas concentration for any general kinetics. The Quantized Method (QM) was presented and used. Using this new strategy for solving coupled partial differential equations (CPDE) permits a great reduction in the mathematical difficulties normally present in gas–solid reaction problems. The authors illustrated the QM's potential by applying it to several gas–solid reaction models, including the grain model (Jamshidi and Ale-Ebrahim, 1996a), half-order model (Jamshidi and Ale-Ebrahim, 1996b), nucleation model (Jamshidi and Ale-Ebrahim, 1997), and the modified grain model (Jamshidi and Ale-Ebrahim, 1999). They included a term to account for the variation of the activation energy with the

progress of reactions, but they assumed a first-order reaction for the gas reactant. Gomez-barea's method (Gómez and Ollero, 2006) can readily overcome this limitation as decided below.

Gómez and Ollero (2006) established a general isothermal model for the reaction:

A(gas) + bB(solid) → cC(gas) + dD(solid)

The model can be written as follows:

$$\varepsilon \frac{\partial C_A}{\partial t} = \frac{1}{r^m} \frac{\partial}{\partial r} \left[r^m D_e \frac{\partial C_A}{\partial r} \right] - (-r_A) \tag{2.33}$$

$$\frac{\partial C_B}{\partial t} = -(-r_B) = -b(-r_A) \tag{2.34}$$

where r_A is the disappearance rate (mol/m^3/s) of gas A, r_B is the disappearance rate (mol/m^3/s) of solid B, D_e is the effective diffusivity of gas (m^2/s), m is the geometric coefficient (m=0: slab, m=1: cylinder and m=2: sphere).

The boundary and initial conditions of the problem are:

$$\text{at} \quad r=L,\ C_A=C_{A,in} \qquad r=0,\ \frac{\partial C_A}{\partial r} = 0 \tag{2.35}$$

$$\text{at} \quad t=0,\ C_A=0 \quad C_B=C_{B0} \tag{2.36}$$

The use of m in Eq. (2.33) allows for the treatment of different geometries. This formulation is applicable to the situations where external mass transfer can be neglected, such as cases with a large Biot number (The Biot number, $\text{Bi}=K_g L / D_e$, is the ratio of internal mass transfer resistance to external mass transfer resistance). When the accumulation term, $\varepsilon(\partial C_A / \partial t)$, in Eq. (2.33) is negligible compared to diffusion and reaction terms, the model is called pseudo-

steady state. The following intrinsic kinetics at any location within the particle is assumed:

$$(-r) = r(C_A)\, F(X) \quad (\text{mol/m}^3\text{-s}). \tag{2.37}$$

The reaction rate has been split into two factors. The first factor, $r(C_A)$, takes into account the effect of gas concentration on reaction rate, while the second, $F(X)$, embodies the effect of the change of available reacting surface. In principle, Eq. (2.37) can accommodate any kinetic model.

In addition, the void fraction or local porosity may change during reaction due to the consumption of solid reactant or the difference between the volume of the solid reactant (B) and product (D). Whatever the case may be, the variation of local porosity (or local conversion) can be modeled by including a given correlation of the effective diffusivity which can be determined experimentally.

An accepted way to do this is to assume the following expression:

$$D_e = D_{e0} g(X). \tag{2.38}$$

The following empirical equation for $g(X)$ was assumed:

$$g(X) = \left(\frac{\varepsilon}{\varepsilon_0}\right)^{\beta} = \left[1 + \frac{(1-\varepsilon_0)}{\varepsilon_0} X\right]^{\beta} \tag{2.39}$$

where $g(X)$ is a function of local porosity, and

D_{e0} is the original (initial) effective diffusivity.

By incorporating Eqs. (2.37) and (2.39) into system (2.33)–(2.36), the following dimensionless set of equations is obtained:

$$\frac{1}{z^m}\frac{\partial}{\partial z}\left[z^m g(X)\frac{\partial C}{\partial z}\right] = \varphi_s^{\,2} F(X) R(C) \tag{2.40}$$

$$\frac{\partial X}{\partial \tau} = F(X)R(C)\,. \tag{2.41}$$

Boundary conditions are given by

$$C\big|_{z=1} = 1\,, \tag{2.42}$$

$$\left(\frac{\partial C}{\partial z}\right)\bigg|_{z=0} = 0\,, \text{ and} \tag{2.43}$$

$$X\big|_{\tau=0} = 1 \tag{2.44}$$

where the following dimensionless variables have been used:

$$z = r / L\,, \tag{2.45}$$

$$\tau = t / \tau_{ref} \tag{2.46}$$

$$C = C_A / C_{A,in} \tag{2.47}$$

$$X = 1 - C_B / C_{B0} \tag{2.48}$$

$$\tau_{ref} = C_{B0} / [b\, r(C_{A,in})] \tag{2.49}$$

$$R(C) = r(C_A) / r(C_{A,in})\,. \tag{2.50}$$

Finally, the parameter:

$$\varphi_s^{\,2} = L^2 \frac{r(C_{A,in})}{D_{e0} C_{A,in}} \tag{2.51}$$

which emerges from Eq. (2.40) is the classical Thiele modulus evaluated at surface conditions.

Once the conversion profile is obtained, the overall particle conversion X_p can be computed by integrating throughout the particle. In dimensionless form, this expression is given by:

$$X_p(\tau) = (m+1)\int_0^1 Xz^m dz \tag{2.52}$$

2.3.3 Approximate solution to Gomez-Ollero's generalized model

Gomez and Ollero's (2006) approximate method is based on the two following steps:

• Step 1: Decoupling of solid and gas conservation equations at a given time.

• Step 2: Using an approximate analytical expression for calculating the gas reactant concentration within an isothermal solid particle at that time. The particle is considered a catalyst with a determined activity distribution. The activity prevailing at a given point of the particle is determined by the local level of conversion at the time considered.

Step 1 is achieved by the application of the QM (Quantized Method). Eq. (2.40) becomes:

$$\frac{1}{z^m}\frac{d}{dz}\left[z^m \frac{\partial C}{\partial z}\right] = \varphi_s^{\,2}(F(X)/g(X))R(C) = M^2(X)R(C) \tag{2.53}$$

$$\varphi_s^{\,2} F(X)/g(X) = M^2(X) \tag{2.54}$$

Boundary conditions are:

$$C\big|_{z=1} = 1, \tag{2.55}$$

$$\left(\frac{\partial C}{\partial z}\right)\bigg|_{z=0} = 0. \tag{2.56}$$

With this method, the concentration profile is given by:

$$C(z) = C^* + (1-C^*)\exp\left\{-\frac{\lambda(1-z^2)}{2-\left[1-zh(z)/(1+2/\lambda)\right]}\right\}. \tag{2.57}$$

Integrating Eq. (2.41) gives:

$$\theta(X) = \tau R(C) = \int_0^x \frac{dX}{F(X)} . \tag{2.58}$$

Rearranging Eq. (2.58) the conversion profile within the particle can be obtained as:

$$X(z) = \theta^{-1}\{\tau R[C(z)]\} \tag{2.59}$$

λ and $h(z)$ in Eq. (2.57) are calculated:

$$IR = \int_0^1 R(C)dC , \tag{2.60}$$

$$M^* = \frac{M}{\sqrt{2IR}(m+1)} , \tag{2.61}$$

$$a = 1 - 4\frac{(m+1)}{(m+3)} IR \cdot R' , \tag{2.62}$$

$$\eta = \left[M^{*2} + \exp(-aM^{*2}) \right]^{-1/2} , \tag{2.63}$$

$$\lambda = \frac{M^2 \eta}{(m+1)(1-C^*)} , \tag{2.64}$$

$$h(z) = \frac{1-\exp(-\lambda z)}{1-\exp(-\lambda)} , \tag{2.65}$$

where C^* is the root of the function $R(C)$ and is zero for most of the kinetic expressions. At a given time the solution of Eqs. (2.57) and (2.59) provides the values of C and X for a given particle position, z. By repeating this procedure for all points of the particle, the profiles of concentration and conversion, $C(z)$ and $X(z)$ are obtained. Once these profiles are available for a given instant, the overall particle conversion is readily computed by means of Eq. (2.52).

The solution of Eqs (2.57)-(2.59) has been performed by dividing the coordinate, z, into $N+1$ points [$z_i = (i-1)\Delta z,\ i = 1{:}\ N+1,\ \Delta z = 1/(N-1)$]. The solution ($C_i$, X_i) is found by solving ($N+1$) systems of two non-linear equations. This has been done by applying the Newton–Raphson method. That means solving:

$$C(z) = C^* + (1-C^*)\exp\left\{-\frac{\lambda(1-z^2)}{2-\left[1-zh(z)/(1+2/\lambda)\right]}\right\} \tag{2.57}$$

$$X(z) = \theta^{-1}\{\tau R[C(z)]\} \tag{2.59}$$

for C and X, then making use of Eq. (2.45) giving X_p.

The requirements for solving the problem are:

(1) the specification of the reaction rate, that is $R(C)$ and $F(X)$

(2) the specification of D_{e0} and $g(X)$

For the previously mentioned three models, $F(X)$ and $\theta(X)$ are:

Unreacted shrinking core model $F(X) = 1-X$ $\theta(X) = -\ln(1-X)$ (2.66)

Grain model $F(X) = (1-X)^{2/3}$ $\theta(X) = 3[1-(1-X)^{1/3}]$ (2.67)

RPM $F(X) = (1-X)[1-\Psi_0\ln(1-X)]^{1/2}$ $\theta(X) = (2/\Psi_0)[1-\Psi_0\ln(1-X)]^{1/2}$ (2.68)

2.4 Determination of the sulfur loading and the breakthrough curve

A breakthrough curve gives an indication of the way in which an adsorbate (H_2S) is distributed within a fixed bed when a gaseous stream containing a fixed percentage of the adsorbate passes through a fixed-bed until the adsorbate emerges in the exit stream. Figure 2.3 (a) shows a typical breakthrough curve. Figure 2.3 (b) shows the concentration of adsorbate in the gas phase at any given point (location) in the bed as a function of time because it results from the

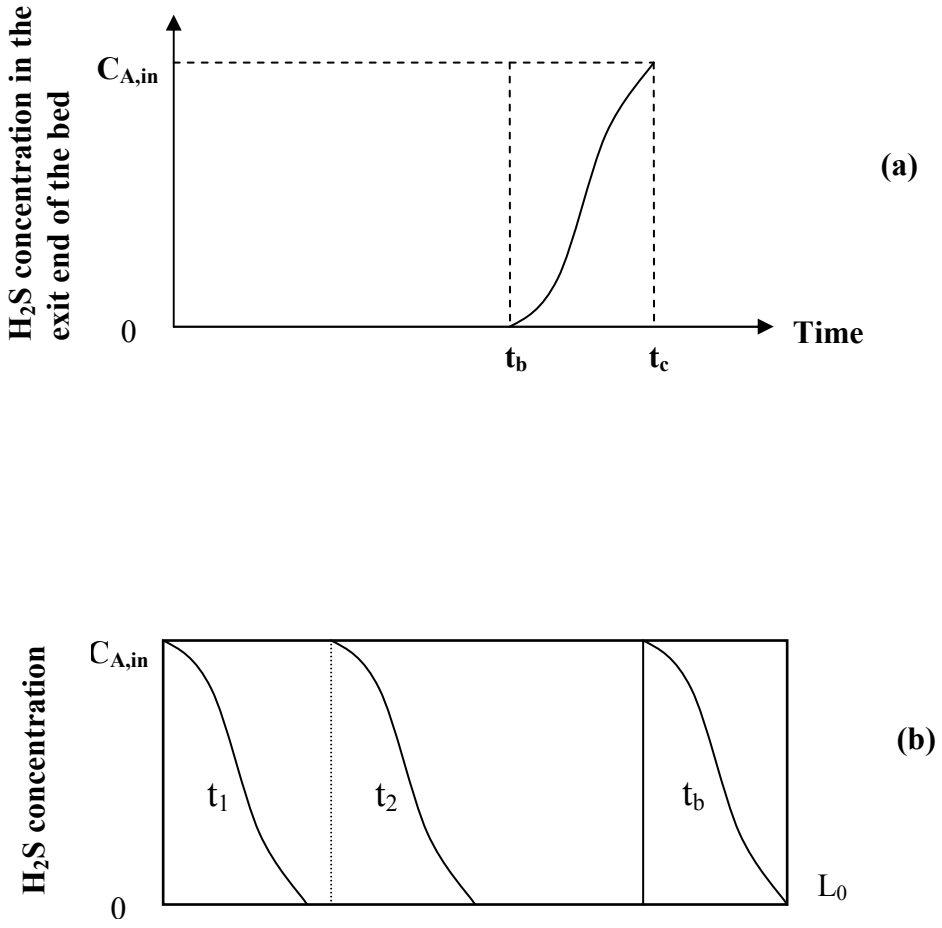

Figure 2.3 Profile of gas phase H_2S concentration in the adsorbent bed:

(a) breakthrough curve from the breakthrough point, t_b, to the complete saturation point t_c.

(b) development and progression of a transition zone along the bed: transition zones at different times t_1, t_2, and breakthrough time t_b;

movement of the concentration front in the bed. On first introducing the gas stream to the bed, the sorbent quickly becomes saturated at the inlet of the bed and the adsorbate concentration falls off rapidly along the bed to form a concentration profile along the bed which is called the transition zone. As the run proceeds, if this concentration profile in the transition zone remains the same, the constant pattern is fully developed and moves in the direction of the gas stream due to the progressive saturation of the adsorption sites at the entrance of the bed. In Figure 2.3 (b) t_1 shows the initial formation of the concentration profile, t_2 shows one at some intermediate time, and t_b shows another just before breakthrough, the point at which the adsorbate H_2S is first detected in the exit stream. After breakthrough the adsorbate concentration in the effluent stream rises steeply up to the value of the inlet concentration during the time interval between t_b and t_c as shown in Figure 2.3 (a).

The shape of the breakthrough curve represents the global adsorption kinetics, and is determined from mass and energy balances on the bed together with the intrinsic adsorption reaction. In most sorption processes, heat transfer effects within the pellet can be neglected. This is because most adsorptive gases are present in an inert carrier gas and their concentrations are small. Also when adsorbates penetrate the porous structure during adsorption and desorption, the local temperature change is negligible. It would be necessary to consider heat transfer effects if the reaction was highly exothermic.

The mass of sulfur adsorbed per mass of adsorbent is called the sulfur loading. The sulfur loading for an adsorbent at breakthrough point was calculated as follows:

$$\text{Sulfur loading} = \frac{V_{H_2S} \times t_b \times C_{A,in} \times MW_S}{W_{fb}} \tag{2.69}$$

where

V_{H_2S} is volumetric rate of feed stream, m^3/s

t_b is breakthrough time, s

$C_{A,in}$ is H_2S concentration, mol/m^3

MW_S is molecular weight of elemental sulfur

W_{fb} is adsorbent loading in the reactor, g.

2.5 Parameters of the breakthrough curve

2.5.1 The stoichiometric time (t_S)

The stoichiometric time is an important parameter for a fixed bed. It is defined as the time needed to reach the total or stoichiometric capacity of the fixed bed. For an iron oxide based fixed bed the stoichiometric time can be calculated from the following expression:

$$t_S = \frac{3 L_0 (1-\varepsilon_{fb}) C_{B0}}{u_g C_{A,in}} \tag{2.70}$$

The stoichiometric time depends on the height of the fixed bed (L_0), the gas superficial velocity (u_g) which is the ratio of volumetric rate of feed storm (V_{H_2S}) to cross sectional area of the fixed-bed, H_2S concentration in the gas streams

($C_{A,in}$), Fe_2O_3 concentration in the adsorbent (C_{B0}) and the fixed-bed porosity (ε_{fb}). The factor of 3 in Eq. (2.70) is due to the 1:3 Fe_2O_3:H_2S stoichiometric ratio in the adsorption reaction, Eq. (2.1).

2.5.2 Mass transfer zone or transition zone (L_t)

The breakthrough curves generally do not appear as step functions. The H_2S concentration from the outlet end of the bed increases from zero to the value of the inlet concentration during a time interval. The H_2S adsorption reaction inside the fixed–bed takes place in the transition zone. If the transition zones maintain a constant pattern, the length of the transition zone, L_t, is calculated with the following equation:

$$L_t = \frac{L_0(t_c - t_b)}{t_S} \tag{2.71}$$

where t_b is the breakthrough time and t_c is the time at which the bed is completely saturated with adsorbate and the outlet adsorbate concentration equals the inlet concentration.

The length of unused bed (*LUB*) at the breakthrough point can be calculated by the fraction of the unused adsorbent in the transition zone:

$$LUB = (1 - t_b / t_S)L_0 \tag{2.72}$$

For a narrow transition zone, the breakthrough curve is very steep and most of the bed capacity is used at the breakthrough point, which means t_b is close to t_S.

If a constant concentration profile in the transition zone is reached as soon as the particles at the very front of the fixed-bed are completely converted, then the

transition zone is fully developed and moves in the direction of the gas stream at a constant velocity u_t, the displacement velocity.

The quantity u_t is given by an overall sulfur mass balance over the reactor bed:

$$\begin{bmatrix}\text{Rate of flow}\\ \text{of } H_2S \text{ to the}\\ \text{fixed}-\text{bed}\end{bmatrix} \quad \begin{bmatrix}\text{Rate of flow}\\ \text{of } H_2S \text{ out of}\\ \text{the fixed}-\text{bed}\end{bmatrix} \quad \begin{bmatrix}\text{Rate of consumption}\\ \text{of adsorbent in the}\\ \text{fixed}-\text{bed}\end{bmatrix}$$

$$\frac{1}{4}\pi D^2 u_g C_{A,in} \quad - \quad 0 \quad = \quad 3\cdot\frac{1}{4}\pi D^2 u_t \cdot (1-\varepsilon_{fb}) C_{B0} \tag{2.73}$$

$$u_t = \frac{u_g C_{A,in}}{3(1-\varepsilon_{fb})C_{B0}} \tag{2.74}$$

It is evident that t_S and u_t have the following relation from Eqs. (2.70) and (2.74):

$$t_S = L_0 / u_t . \tag{2.75}$$

2.5.3 Residence time (t_r)

Residence time is the retention time of the reacting gas in the reactor. When the plug flow assumption is acceptable the residence time of the reacting gas (at standard state 0 ºC and 1 atm) in an empty reactor is:

$$t_r = L_0 / u_g \tag{2.76}$$

Plug flow is a simplified and idealized situation where all the fluid elements move with a uniform velocity. Otherwise, the above expression is the mean residence time for the gas in the fixed-bed reactor.

2.5.4 Mass flux of H_2S

Mass flux of H_2S is calculated as follows:

$$\text{Mass flux of } H_2S = u_g \times C_{A,in} \times MW_{H_2S} \tag{2.77}$$

The mass flux of H_2S in the feed stream has a unit of mass of H_2S per unit time per unit cross sectional area of the bed and depends on the superficial velocity (u_g) at the inlet of the bed and H_2S concentration ($C_{A,in}$) in the feed stream, and represents the strength of H_2S in the feed gas stream.

2.6 Conversion profiles from breakthrough curves

A sulfur mass balance on a differential cross-section of the bed shown in Figure 2.4 yields:

$$\frac{1}{4}\pi D^2\, dZ\, \varepsilon_{fb} \frac{\partial C_A}{\partial t} = \frac{1}{4}\pi D^2\, u_g\, C_A\big|_Z - \frac{1}{4}\pi D^2\, C_A\big|_{Z+dZ} - 3 \cdot \frac{1}{4}\pi D^2\, dZ \left(1-\varepsilon_{fb}\right) C_{B0} \frac{\partial X}{\partial t} \tag{2.78}$$

$$\varepsilon_{fb} \frac{\partial C_A}{\partial t} = \left(u_g\, C_A\big|_Z - u_g\, C_A\big|_{Z+dZ}\right) / dZ - 3\left(1-\varepsilon_{fb}\right) C_{B0} \frac{\partial X}{\partial t} \tag{2.79}$$

$$\varepsilon_{fb} \frac{\partial C_A}{\partial t} = -u_g \frac{\partial C_A}{\partial Z} - 3\left(1-\varepsilon_{fb}\right) C_{B0} \frac{\partial X}{\partial t} \tag{2.80}$$

The following variable transformation can be performed using the method proposed by Fenouil and Lynn (1996)

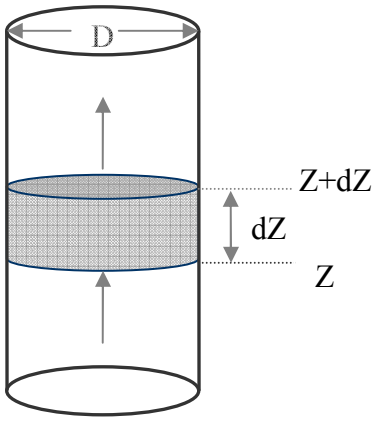

Figure 2.4 A differential cross-section of the bed

$$\tau = t - Z / u_t , \tag{2.81}$$

$$Z = (t - \tau) u_t , \tag{2.82}$$

resulting in

$$\frac{\partial C_A}{\partial \tau} = \frac{dC_A}{d\tau} , \tag{2.83}$$

$$\frac{\partial X}{\partial t} = \frac{dX}{d\tau} , \text{ and} \tag{2.84}$$

$$\frac{\partial C_A}{\partial Z} = -\frac{1}{u_t} \frac{dC_A}{d\tau} . \tag{2.85}$$

By incorporating Eqs. (2.83-2.85) into Eq. (2.80) the following equation is obtained:

$$\varepsilon_{fb} \left(1 - \frac{u_g}{\varepsilon_{fb} u_t} \right) \frac{dC_A}{d\tau} + 3 C_{B0} (1 - \varepsilon_{fb}) \frac{dX}{d\tau} = 0 \tag{2.86}$$

where the boundary conditions are

$$C_A = C_{A.in} \text{ and } X = 1 \text{ at } \tau = 0. \tag{2.87}$$

for the moment of complete conversion of the adsorbent at outlet end.

Integration of Eq. (2.86) gives:

$$\varepsilon_{fb} \left(1 - \frac{u_g}{\varepsilon_{fb} u_t} \right) (C_A - C_{A,in}) + 3 C_{B0} (1 - \varepsilon_{fb}) (X - 1) = 0 \tag{2.88}$$

Substituting Eq. (2.74) into Eq. (2.88) gives (Fenouil and Lynn, 1996):

$$C_A = C_{A,in} \frac{X - \frac{u_t \varepsilon_{fb}}{u_g}}{1 - \frac{u_t \varepsilon_{fb}}{u_g}} \tag{2.89}$$

which shows the relationship between C_A and X at any point of the breakthrough curve. Rearranging Eq. (2.89) gives:

$$\frac{C_A}{C_{A,in}} = \frac{X - \frac{u_t \varepsilon_{fb}}{u_g}}{1 - \frac{u_t \varepsilon_{fb}}{u_g}} \tag{2.90}$$

which shows that the data, $C_A / C_{A,in}$, at the outlet end of fixed bed with time can be related to X with time t.

In this chapter, some background information and technologies for sulfur removal from gas streams were introduced. The models for gas-solid adsorption reactions and their solutions were reviewed. The measurement and analysis of breakthrough curve were covered. The following two chapters are based on this chapter.

Chapter 3

Experimental Methods

This chapter describes the experimental material suppliers, set-up, procedure, and analysis of the effluent gas from the fixed-bed. The experimental parameters were chosen in terms of the operating conditions of natural gas processing plants, including pressures of 4-50 atm absolute (all pressures in this work are absolute pressures), superficial velocities of 0.09-0.26 m/s, and H_2S concentrations of 0.50-6.01% v/v.

3.1 Material suppliers

CG-4 was supplied by CLEAN Catalysis and Purification Technologies Development Company in Shanxi Province, China. The gas mixture, 6.01% v/v H_2S and balance N_2, was provided by Praxair. A cylinder of nitrogen (Praxair) was used to dilute the gas mixture to the desired concentration of H_2S. The ammonia cylinder was anhydrous liquid ammonia with a purity of 99.99% w/w (Praxair).

3.2 Experimental set-up

The experiment is carried out at various pressures, in the range of 4 - 50 atm absolute, and at room temperature (21~23 ºC) in a fixed-bed reactor. The fixed-bed reactor is a 600 mm long, 11 mm ID, 316 stainless steel tube. Fig 3.1 shows the schematic diagram of the experimental set up which consists of a gas feed system, fixed-bed reactor, an on-line GC, and a data acquisition computer.

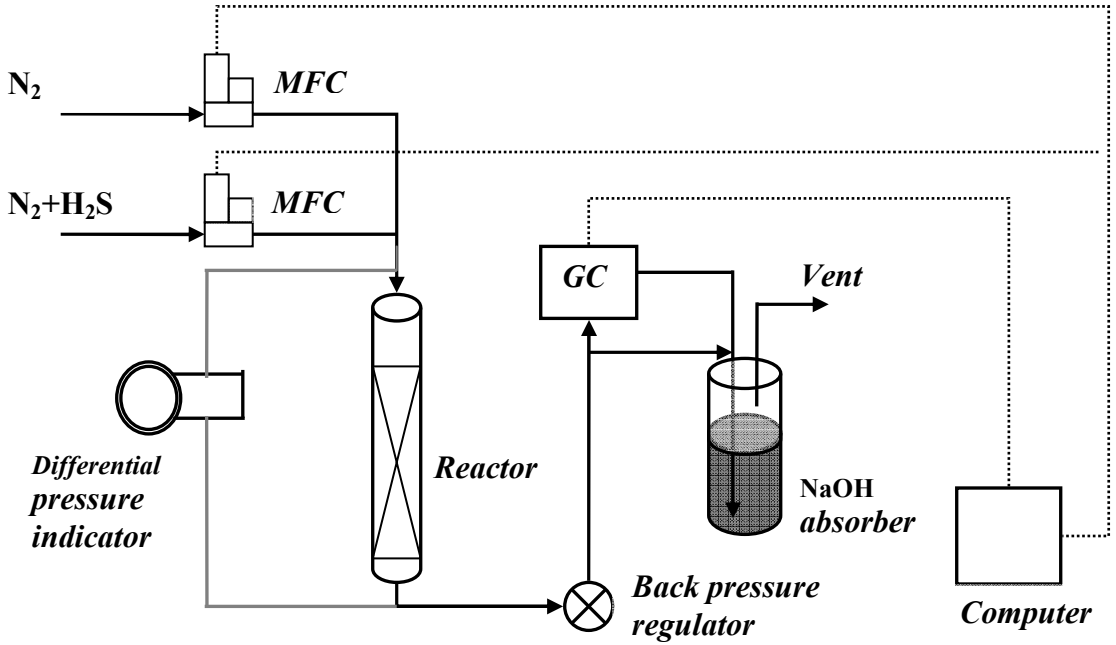

Figure 3.1. Schematic diagram of experimental setup

The flow rates of the gases are controlled by mass flow controllers (5850S smart mass flow, Brooks instruments Inc.). The accuracy of these controllers is ±0.7% of the rate. The calibrations curves are shown in Appendix C. The reactor pressure is adjusted by a back pressure regulator (Swagelok) located at the gas exit line and it is measured using the differential pressure indicator (SCADASENSE 4102, Control Microsystems), the accuracy of which is ±0.05% of its span. The H_2S concentration at the exit gas line was measured by the on-line 6890N Network GC System coupled with thermoconductivity detector (TCD) which has a minimum detection limit of 100 ppm for H_2S, and flame photometric detector (FPD) which has a minimum detection limit of 10 ppm for H_2S (Agilent technologies).

The setup for ammonia leaching is simple. The flow rate of liquid ammonia is controlled by a needle valve. The leaching vessel is a 316 stainless tube, 600 mm in length and 22 mm in I.D. The pressure of the vessel is adjusted by a back pressure regulator preventing the liquid ammonia from vaporization.

3.3 Experimental Procedure

A measured amount of iron oxide adsorbent is loaded into the reactor. The operating pressure is set using the pressurized nitrogen gas stream and adjusting the back pressure regulator. Once the pressure stabilizes, the H_2S mixture gas, which has a known concentration, is fed into the reactor. Nitrogen is used as a balance gas to dilute the H_2S mixture gas to a desired H_2S concentration. The breakthrough curves are obtained from the measurements of H_2S concentration at the outlet end of the reactor.

3.4 Analysis of effluent gas from the fixed-bed

There are several configurations for combining the TCD (thermal conductivity detector) and FPD (flame photometric detector) within a single GC. The first option is to place them in series after a single column. The other option is to arrange them in parallel, where each of the detectors senses a sample from different GC columns. The first option was adopted in this study. Due to the large difference in the sensitivity for sulfur between the TCD and the FPD, the key to accuracy is that the transition from FPD to TCD must be timed carefully. The H_2S concentration of effluent from the fixed-bed reactor gradually increases after the breakthrough time. At the beginning of breakthrough (H_2S 50-500 ppm) the FPD may get valid readings and a good GC peak for sulfur, meanwhile the TCD may not get any response. At a certain time after breakthrough, when the H_2S concentration of effluent is within the range of 600 ppm-1000 ppm, both of detectors have good responses. When H_2S concentrations are more than 1000 ppm the FPD is overloaded and the peak tops are flattened and tailed. During the testing of the experiment, when the low concentrations of H_2S in the effluent exist the FPD is used, otherwise the TCD is used. The operating parameters for GC and detectors are listed in Table 3.1.

The calibration for detectors was carried out by using known concentrations of H_2S mixture gases. The calibration curves and calibration equations for TCD and FPD are shown in appendices A and B. Three typical sample uncertainties in calibrations respectively for the TCD and the FPD in terms of 95 % confidence

Table 3.1 Operating parameters for GC and detectors

Description	**Value**
Oven temperature program	Ramp to 120 °C at 20 °C/min; held for 5 minutes
Capillary column	60.0 m x 320 µm x 0.00 µm nominal
Split ratio	5.0:1
split flow rate	28.2 mL/min
TCD detector	
Heater temperature	250 °C
reference flow (Helium)	20 mL/min
Makeup flow (Helium)	7.0 mL/min
FPD detector	
Heater temperature	200 °C
H_2 flow rate	75 mL/min
Air flow rate	100 mL/min
Makeup flow rate (Nitrogen)	15.0 mL/min

intervals are listed in Table 3.2. Those data show that the errors are mainly caused by the calibrations for the TCD and FPD.

Table 3.2 95% confidence intervals in calibrations for the TCD and the FPD

Detector	TCD			FPD		
Area	1820.00	801.32	316.72	696160	616570	247000
Concentration (ppm)	60100 ± 800	30050 ± 450	12020 ± 350	1040 ± 46	858 ± 42	347 ± 24

Chapter 4

Results and Discussion

This chapter describes and discusses the results obtained from different experimental studies. The results of the adsorption experiments for three adsorbent samples are given in section 4.1. Section 4.2 describes the reproducibility of the data with the experimental set-up and procedures. Section 4.3 describes the breakthrough behaviors for the selected adsorbent under different conditions. The change in sulfur loadings under different operating conditions are discussed in section 4.4. Pressure drop over the fixed-bed and breakthrough behaviors for the regenerated adsorbents are discussed in section 4.5 and section 4.6 respectively. Section 4.7 describes the regression analysis of the breakthrough behaviors.

4.1 The screening of adsorbent samples for CG-4A, CG-4B and CG-4C

Three adsorbent samples denoted as CG-4A, CG-4B and CG-4C were obtained from the manufacturer, CLEAN Catalysis and Purification Technologies Development Company in Shanxi Province, China. The adsorbent particles were brown, cylindrical granules, 2 mm in diameter and 3-4 mm in length.

The properties of these samples are shown in Table 4.1, which was provided in the product manual by the manufacturer. The adsorption experiments were performed at an absolute pressure of 10 atm, a superficial velocity of 0.022 m/s (0°C and 1 atm) (volumetric flow rate 500 mL/min), an inlet H_2S concentration of

Table 4.1 Chemical and physical characteristics of CG-4 adsorbents

Properties	CG-4A	CG-4B	CG-4C
Packing density (g/cm^3)	0.73	0.56	0.66
Pore volume (mL/g)	0.36	0.34	0.46
Voidage (%)	55	57	47
Fe_2O_3 content (% w/w)	54.8	28.7	63.4
H_2O content (% w/w)	11.0	15.5	13.8

Source: manufacturer manual

6.01% v/v, and a bed height of 24.5 cm. At the breakthrough points the sulfur adsorption loadings, or sulfur loadings were 18.79% w/w, 5.66% w/w, and 22.23% w/w for CG-4A, CG-4B, and CG-4C respectively. CG-4C has the largest sulfur loading. This result is logical because the sulfur loading of the sample is proportional to its total content of Fe_2O_3, the active component in CG-4 adsorbent.

CG-4C was chosen as the adsorbent to test the breakthrough curve behavior unless otherwise noted.

4.2 Reproducibility of the data

The reproducibility of the data with an experimental setup and procedures is critical to the accuracy of research. Therefore, five experiments of sulfur loading measurement were performed at the same conditions: a bed height of 24.5 cm (CG-4C adsorbent loading 16 g), superficial velocity of 0.26 m/s, and H_2S inlet concentration of 3.00% v/v. Figure 4.1 shows the breakthrough curves of the five runs of experiments. A statistical analysis of sulfur loadings from the five repeated experiments was performed giving a sulfur loading 23.3% ± 0.6% w/w. Detailed results are listed in Table 4.2. Given the 4 degrees of freedom a Student $t_{0.975}$ value of 2.78 was used to calculate the confidence interval at the 95% probability level. In this work, uncertainties were analyzed by using the Student t test at the 95% probability level.

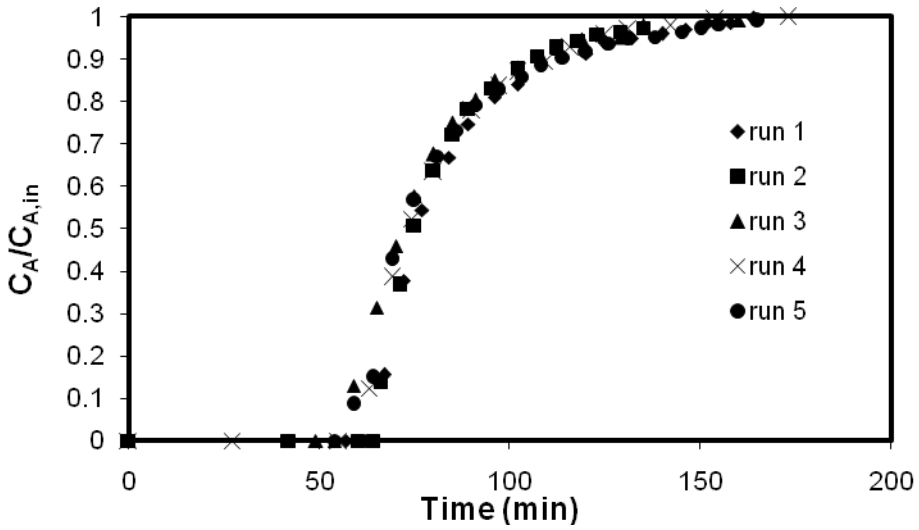

Figure 4.1 The breakthrough curves for the reproducibility experiments at the conditions: $L_0 = 24.5$ cm; $u_g = 0.26$ m/s; $C_{A,in} = 3.00$ % v/v.

Table 4.2 The data statistics for five experiments of sulfur loading measurement

Run Number	1	2	3	4	5
Sulfur loading (% w/w)	23.03	23.63	22.84	24.01	22.96
Average sulfur loading (% w/w)			23.29		
Standard deviation			0.5		
Relative standard deviation			2.16 %		

4.3 Breakthrough behaviors

As stated in Chapter 2, the breakthrough curves do not appear like a step function because the adsorption reaction rate is finite. The H_2S concentration in the outlet gas stream increases from zero to the value that is equal to the inlet H_2S concentration during a time interval between the breakthrough time (t_b), at which the H_2S first shows in the effluent gas, and the complete saturation time (t_c), at which the H_2S concentration in the effluent gas becomes equal to the H_2S inlet concentration. The axial changes in H_2S concentration and adsorbent conversion take place in the transition zone. The shape of the breakthrough curve gives an indication of the apparent adsorption kinetics which is determined by the operating conditions. The effects of changing H_2S inlet concentration, operating pressure, and gas flow superficial velocity on the adsorption kinetics and the shape of the breakthrough curves are investigated as follows.

4.3.1 Effect of changing inlet H_2S concentration

Several experiments were carried out with different H_2S concentrations ranging from 0.50% to 6.01% v/v, at room temperature (21~23 °C) and 50 atm as shown in Figure 4.2. The aim was to study the effect of H_2S inlet concentration on the breakthrough curve and sulfur loading and to estimate the effect of H_2S feed concentration on the adsorption reaction.

At a constant total operating pressure of 50 atm, the slope of the breakthrough curve lessens and the period of time between t_b and t_c increases, when the inlet H_2S concentration in gas is decreased. The complete saturation time, t_c, was not obtained in a typical experiment run time when the H_2S inlet

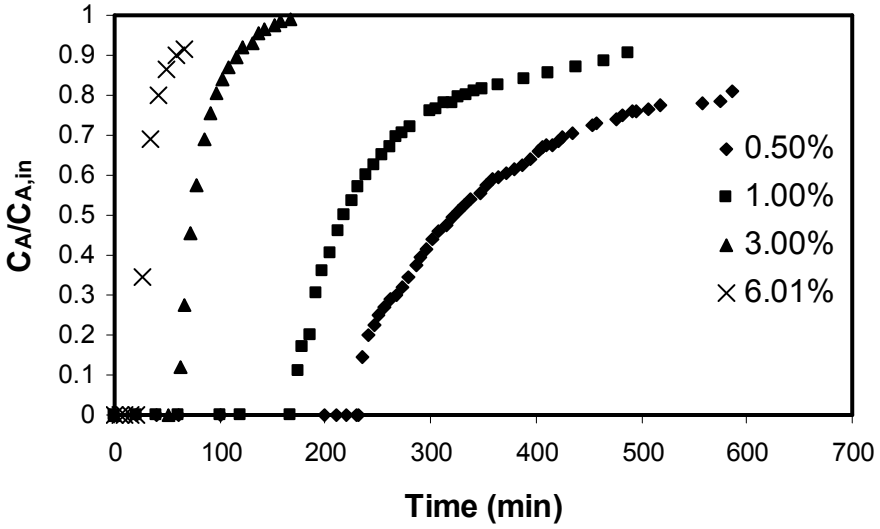

Figure 4.2 Effect of H_2S concentration on breakthrough at P = 50 atm, L_0 = 24.5 cm; u_g = 0.26 m/s.

concentration was below 1.00% v/v. As a result, the transition zone, or working zone, in the fixed-bed becomes longer at lower inlet H_2S concentrations. It is understood that lower apparent reaction rate between H_2S and the adsorbent results in a longer working zone (Adanze, 2005). Therefore, lower H_2S inlet concentration in a gas leads to lower apparent reaction rate. Furthermore, as the H_2S concentration decreases, a longer bed, or more active sites, is needed to consume a given amount of H_2S within the same time period.

4.3.2 Effect of change in operating pressure

An investigation into the effect of the total operating pressure on the breakthrough curves for adsorbent CG-4C was conducted. Figure 4.3 shows the breakthrough curves for various total pressures at a constant H_2S concentration of 3.00% v/v.

It was found that the breakthrough curves show no obvious change when the total pressure was changed from 4 atm to 50 atm at 3.00% v/v H_2S. It is known that the increase in total pressure will lead to an increase in the H_2S partial pressure when the H_2S inlet concentration is the same. The increase in H_2S partial pressure should results in a more rapid adsorption reaction according to either reaction kinetics or mass transfer laws. To verify this hypothesis, another set of experiments were performed where the H_2S partial pressure was kept constant of 0.15 atm by varying the total pressure and the H_2S inlet concentration simultaneously. It was hypothesized that by doing so the same shape of breakthrough curves would be observed because the same H_2S partial pressure

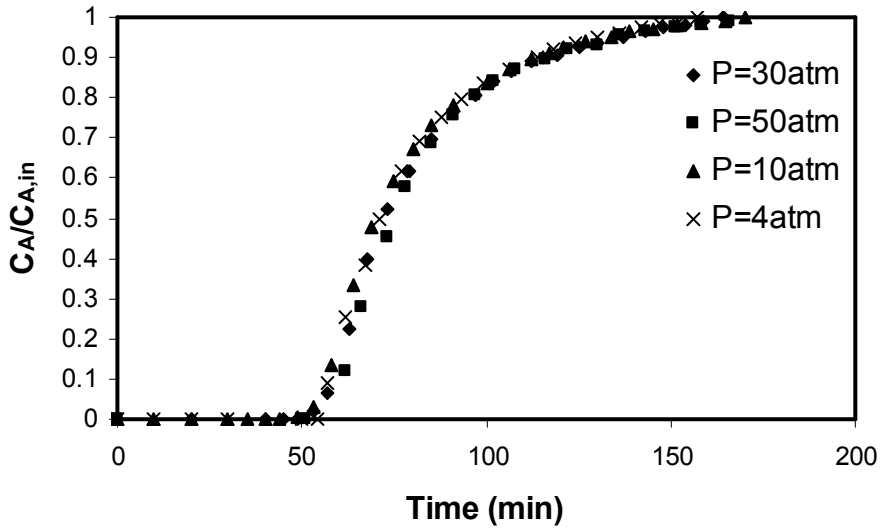

Figure 4.3 Effect of changing pressures on the breakthrough curves at $C_{A,in}$ 3.00 % v/v, L_0 = 24.5 cm; u_g = 0.26 m/s.

should results in the same adsorption reaction. However, the results shown in Figure 4.4 do not prove the hypothesis. Figure 4.4 shows a similar trend to that seen in Figure 4.2 for changes in the H_2S inlet concentration. There seems to be no correlation with change in pressures. Other researchers attempted to explain the effect of total pressure change in their gas-solid systems. Qiu and Lindqvist (2000) used the unreacted shrinking core model to describe the sulfidation reaction of CaO with SO_2. The kinetic rate constant they determined decreases as total pressure increases. Garcia-Labiano (2004) applied the grain model to predict the direct sulfidation of half-calcined $CaCO_3$·MgO by H_2S. They found that the pre-exponential factor of the Arrhenius-type reaction rate constant becomes less when total pressure is higher but the activation energy does not change with total pressure. Nevertheless, the conclusion drawn from this research tends to be that total pressure change in gas phase does not change the breakthrough curve characteristics when other operating conditions are kept the same.

4.3.3 Effect of fixed-bed length change

When other operating parameters such as the total pressure, the H_2S inlet concentration, and the gas superficial velocity were kept the same, it was observed that the breakthrough curves obtained with different bed lengths (different adsorbent loadings of 8 g, 12 g, and 16 g) are closely shaped as shown in Figure 4.5. This observation indicates that the global reaction dynamic does not change due to the change in bed length and therefore fully developed flow has been established within the first 11.5 cm of the bed (Froment and Bischoff, 1990). The

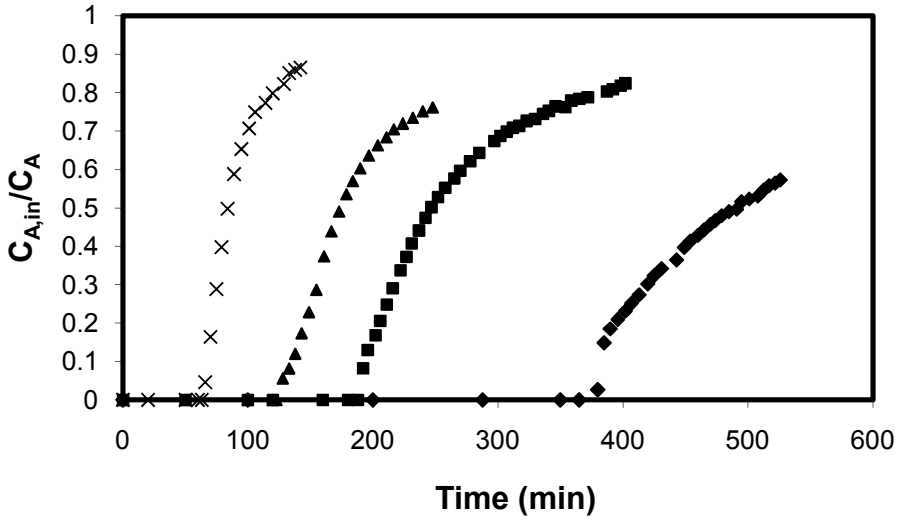

Figure 4.4 Effect of total pressure on the breakthrough curves at a constant H_2S partial pressure of 0.15 atm (×: P = 5 atm, $C_{A,in}$ = 3.00 v/v; ▲: P = 10 atm, $C_{A,in}$ = 1.50 % v/v; ■: P = 15 atm, $C_{A,in}$ = 1.00 % v/v; ♦: P = 30 atm, $C_{A,in}$ = 0.50 % v/v).

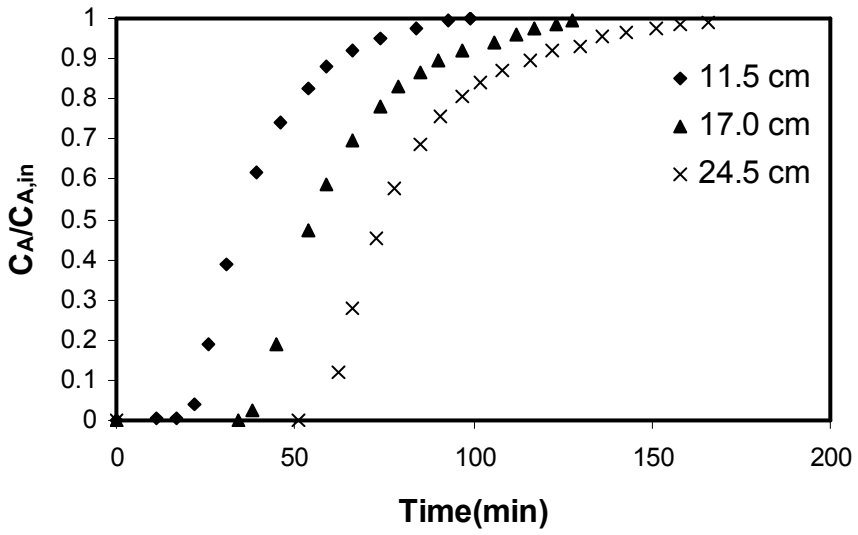

Figure 4.5 Effect of the bed height on the breakthrough curves at P = 50 atm, $C_{A,in}$ = 3.00 % v/v, u_g = 0.26 m/s.

longitudinal Peclet number, Pe, shows the ratio of the rate of transport by convection to the rate of transport by dispersion. Under the experimental condition for the shortest bed length:

$$\mathrm{Pe} = \frac{u_g L_0}{D_{H_2S}} = \frac{0.0052 \times 0.115}{1.09 \times 10^{-8}} = 5.49 \times 10^4 . \quad (4.1)$$

According to Fogler (2006), plug-flow can be assumed when Pe is larger than 1000, strongly suggesting that plug flow conditions exist within experiments conducted. It is noted that $D_{\mathrm{H_2S}}$ was calculated using Fuller's method (Poling et al. 2001):

$$D_{\mathrm{H_2S}} = \frac{4.52 \times 10^{-4}\, T^{1.75}}{P\left[2(MW_{\mathrm{N_2}}{}^{-1} + MW_{\mathrm{H_2S}}{}^{-1})^{-1}\right]^{0.5} \left[(\Sigma\nu)_{\mathrm{N_2}}{}^{1/3} + (\Sigma\nu)_{\mathrm{H_2S}}{}^{1/3}\right]^2} . \quad (4.2)$$

For the H_2S-N_2 system: $MW_{\mathrm{H_2S}} = 34$, $MW_{\mathrm{N_2}} = 28$, $(\Sigma\nu)_{\mathrm{N_2}} = 18.5$, $(\Sigma\nu)_{\mathrm{H_2S}} = 27.52$ at $T = 296$ K, and $P = 50$ atm.

4.3.4 Effect of superficial velocity change

At an identical total gas pressure of 50 atm, and the same H_2S inlet concentration of 3.00% v/v, the effect of changing superficial gas velocity was studied. From Figure 4.6 it can be seen that the breakthrough curves appeared at later times as the gas superficial velocity decreased. This is because the mass flux of H_2S in inlet end of the bed decreases and therefore the stochiometric time increases according to Eq. (3.6). In addition, the shape of the breakthrough curves became less steep with a decrease in gas superficial velocity as shown in Figure

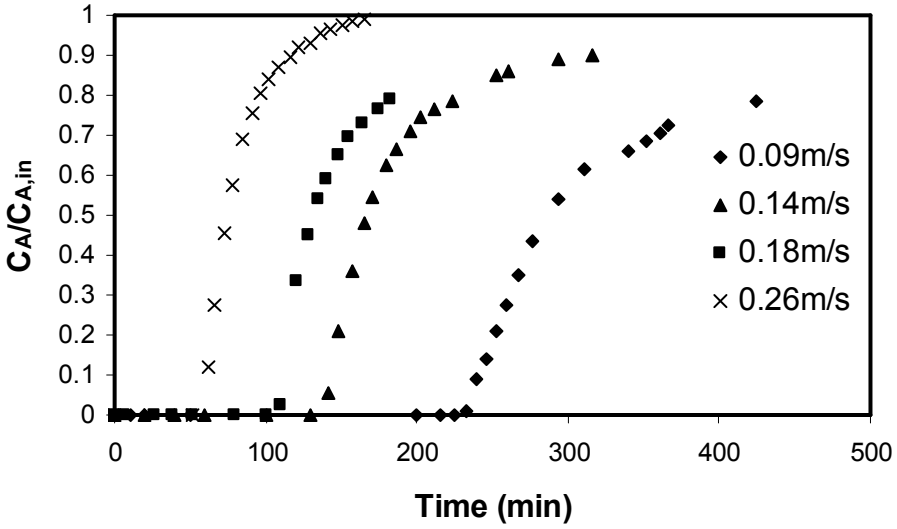

Figure 4.6 Effect of superficial velocity on breakthrough curves at P = 50 atm, $C_{A,in}$ = 3.00 % v/v.

4.7. This means that the global reaction rate decreases with a decrease in superficial velocity and therefore it shows that the mass transfer resistance in the gas film was not negligible under the operating conditions used.

4.3.5 Effect of the addition of methane to the H_2S-N_2 mixture

Methane is the main component in natural gas. Whether methane (CH_4) affects the breakthrough behavior of H_2S in adsorbent bed was studied by adding methane to the gas mixture. The shape of the breakthrough curves at different concentrations of methane in the gas mixture, having the same inlet H_2S concentration of 3.00% v/v, are similar to each other as seen in Figure 4.8. It can be also seen in Figure 4.8 that the change in total pressure has no effect on the breakthrough curves and sulfur loadings even when CH_4 is present. Two experiments were also performed at the same inlet H_2S concentration of 1.00% v/v and at the same pressures of 5 atm, but one of them was performed for a H_2S – CH_4 mixture containing 50% v/v methane, the other for a H_2S-N_2 mixture without methane. Figure 4.9 indicates that the presence of methane in the H_2S-N_2 mixture does not has an impact on the breakthrough curve and sulfur loading. Therefore it is concluded that the CG-4 adsorbent shows the same, or at least, the very similar breakthrough behavior for either a H_2S-N_2 or a H_2S-CH_4 mixture.

4.4 Sulfur loadings of adsorbent under different operating conditions

Sulfur loading is the intake capacity of H_2S for an adsorbent, it can be calculated by Eq. (2.57) after the breakthrough time, t_b, is measured by an

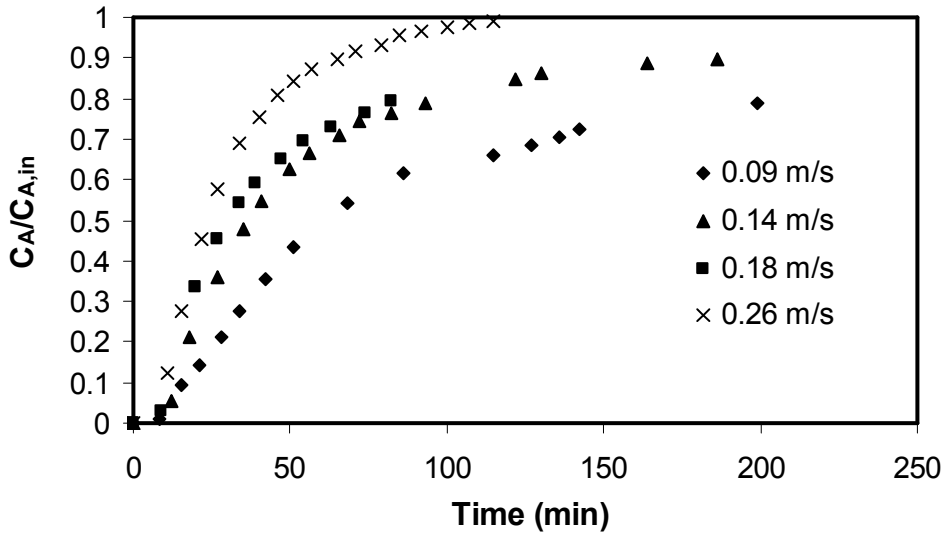

Figure 4.7 Comparison of the shapes of breakthrough curves for different superficial velocities at P = 50 atm, $C_{A,in}$ = 3.00 % v/v.

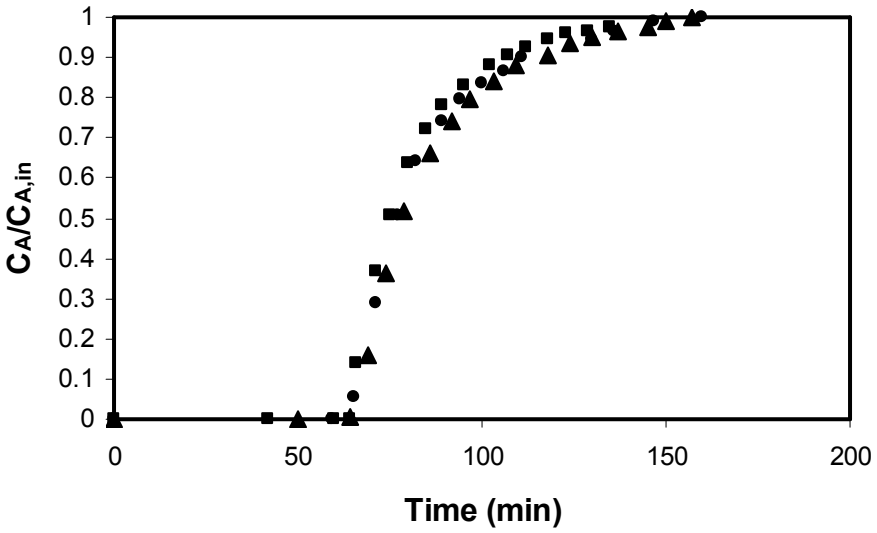

Figure 4.8 Comparison of effect of methane in the mixture gas with inlet H_2S concentration 3.00 % v/v at different experimental conditions. (▲20 atm, 50.00 % v/v CH_4; ■ 5 atm, 0.00 % v/v CH_4; ● 5 atm, 50.00 % v/v CH_4)

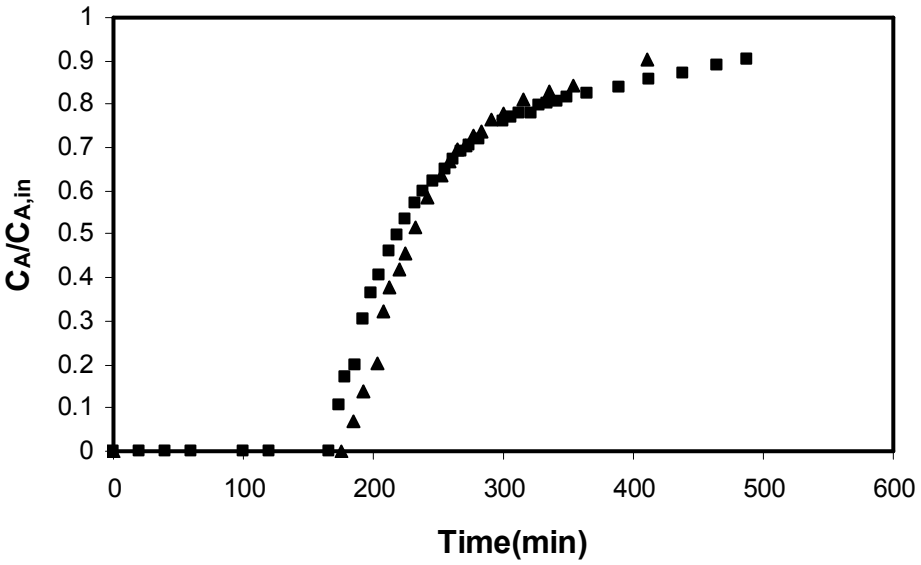

Figure 4.9 Comparison of effect of methane in the mixture gas with inlet H_2S concentration 1.00 % v/v at different concentrations of CH_4. (▲5 atm, 83.30 % v/v CH_4; ■ 5atm, 0 % v/v CH_4)

experiment under certain operating conditions such as inlet H_2S concentration, $C_{A,in}$, operating pressure, P, superficial velocity, u_g, bed height, L_0.

4.4.1 Effect of change in inlet H_2S concentration

The sulfur loadings at different H_2S feed concentrations are listed in Table 4.3, experiments 5 to 8. The sulfur loading decreases while the H_2S concentration increases from 0.50% to 6.01% v/v. It is assumed that adsorbent pellets have finished reacting when the breakthrough point is observed. However, incompletely reacted cores exist inside the adsorbent pellets in saturated bed zone. This is because the mass transfer resistance in the reacted layer of the adsorbent become so large that the reaction rate is insignificant compared with that in the main working zone of the bed. The size of these cores increase and therefore the sulfur loading decreases with the increase of the H_2S concentration in the feed stream. This is because the moving velocity of transition zone increases and therefore reacting time decreases. The mass flux of H_2S in the feed stream is used to indicate this impact of H_2S inlet concentration on the adsorption process, as shown in Figure 4.10. It is shown that when the mass flux of H_2S in the feed stream is less then 11.3 g/m^2-s, its impact on sulfur loading is negligible.

4.4.2 Effect of change in operating pressure

When the total pressure was changed from 4 atm to 50 atm at a H_2S concentration of 3% v/v, the sulfur loading remained constant at about 23% w/w. When the partial pressure of H_2S was maintained at 0.15 atm and the total

Table 4.3 The results of the experiments performed using the fixed-bed at 50 atm

Exp	u_g (m/s)	$C_{A,in}$ (% v/v)	L_0 (cm)	t_r (s)	t_b (min)	t_s (min)	LUB (cm)	FUB (%)	SC (% w/w)
1	0.09	3.00	24.5	2.8±0.2	225±1	260±17	3.0±0.2	12.3±0.9	30.1±0.4
2	0.14	3.00	24.5	1.8±0.1	135±1	160±8	3.9±0.2	15.8±0.8	28.9±0.3
3	0.18	3.00	24.5	1.4±0.1	101±1	128±9	5.2±0.4	21.2±1.6	27.1±0.3
4	0.26	3.00	24.5	0.94±0.03	60±1	85±3	7.3±0.3	29.8±1.2	22.9±0.4
5	0.26	0.50	24.5	0.94±0.03	369±1	510±10	6.9±0.1	28.2±0.4	24.7±0.2
6	0.26	1.00	24.5	0.94±0.03	166±1	257±3	8.6±0.1	35.4±0.4	22.8±0.2
7	0.26	3.00	24.5	0.94±0.03	60±1	85±3	7.3±0.3	29.8±1.2	22.9±0.4
8	0.26	6.01	24.5	0.94±0.03	20±1	43±2	13.0±1.0	53.2±4.0	16.1±0.8
9	0.26	3.00	11.5	0.44±0.02	10±1	40±2	8.6±1.0	75.1±8.7	8.0±0.8
10	0.26	3.00	17.0	0.65±0.03	34±1	59±4	7.3±0.9	42.7±5.3	18.2±0.5

1. FUB, fraction of unused bed. 2. SC, Sulfur loading; 3. t_r, residence time.

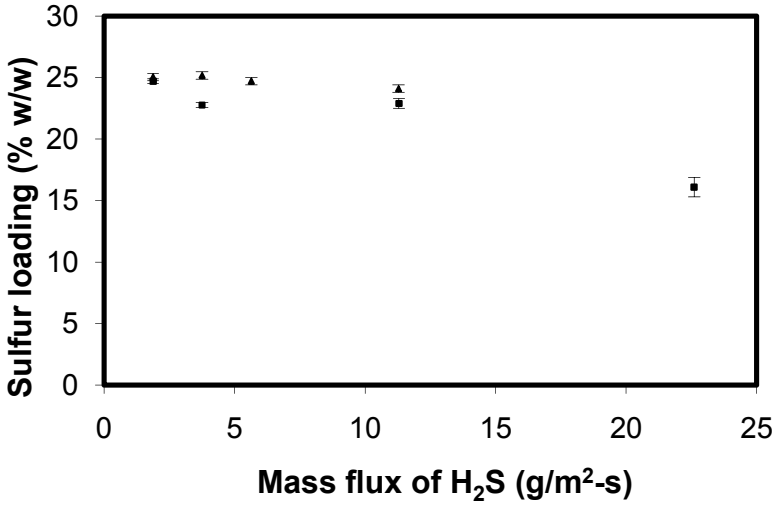

Figure 4.10 Effect of mass flux of H_2S on sulfur loading at u_g = 0.26 m/s and L_0 = 24.5 cm. ▲ Data from the experiments on pressure (P=5, 10, 15, 30 atm). ■ Data from the experiments on concentration at same residence time ($C_{A,in}$ = 6.01, 3.00, 1.00, 0.50% v/v).

pressure was changed, there was no significant difference in the sulfur loading (see Figure 4.10), although there are different shapes of breakthrough curves (see Figure 4.4). It can be concluded that the impact of total pressure on sulfur loading is not significant.

4.4.3 Effect of change in superficial velocity and height of the bed

As shown in Figure 4.11, when the superficial gas velocity increased, the sulfur loading at the breakthrough point decreased. The reason for this is that the residence time decreased. The change in height of bed also changes the residence time and has the same impact on sulfur loading. This is why these two parameters are discussed together.

The sulfur loading changes as shown in Figure 4.12 with the change in residence time. The rate of change decreases as the residence time increases. When the residence time is more than 3 seconds, the impact of a change in residence time on the sulfur loading is negligible.

4.5 Pressure drop in the fixed-bed

The pressure drop of the CG-4 adsorbent bed in the breakthrough curve experiments was monitored. The Ergun, Hukill and Shedd equation (McGuckin, 1999), correlating pressure drop, ΔP, with gas viscosity, density, porosity of the bed, sphericity of adsorbent particles, and particle diameter, was used to evaluate the experimental ΔP. The equation is

$$\frac{\Delta P}{L_0} = 150 \frac{u_0 \mu_g (1-\varepsilon_{fb})^2}{\psi_s^{\,2} d_p^{\,2} \varepsilon_{fb}^{\,3}} + 1.75 \frac{u_0^{\,2} \mu_g (1-\varepsilon_{fb})}{\psi_s d_p \varepsilon_{fb}^{\,3}} \tag{4.3}$$

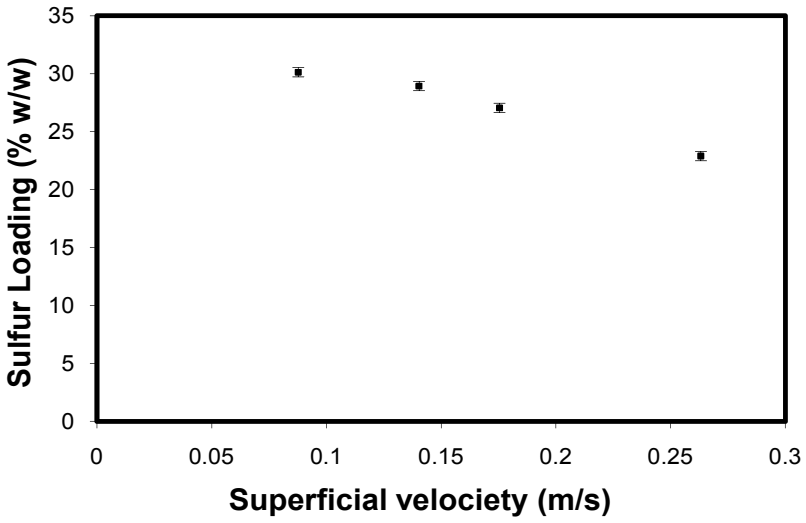

Figure 4.11 Effect of superficial velocity on sulfur loading at P = 50 atm, $C_{A,in}$ = 3.00% v/v. (experiments 1-4 in Table 4.3)

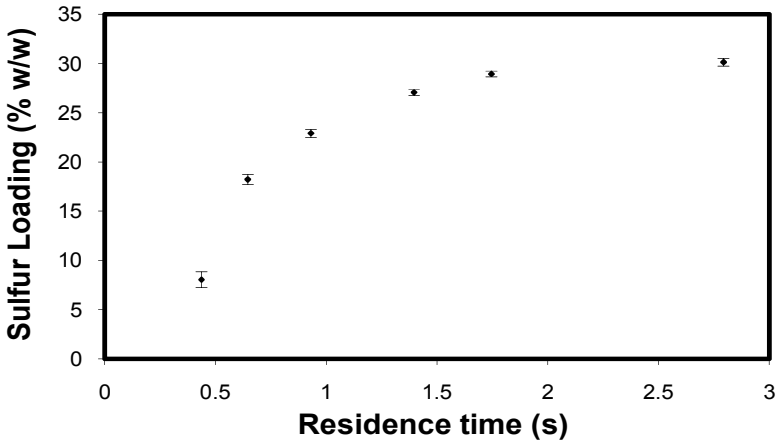

Figure 4.12 Effect of changing residence time on sulfur loading (Experimental conditions are shown in experiments 1-4 and 9-10 in Table 4.3)

where sphericity, ψ_S, of a particle is the ratio of the surface area of a sphere (with the same volume as the given particle) to the surface area of the particle. For a cylindrical particle:

$$\psi_s = \frac{\pi^{\frac{1}{3}} * (6 * V_P)^{\frac{2}{3}}}{A_P} = \frac{\pi^{\frac{1}{3}} * (6 * \pi r^2 * h)^{\frac{2}{3}}}{2\pi r^2 + 2\pi r h} \tag{4.4}$$

Table 4.4 shows the values of experimental pressure drop in the adsorbent bed. Figures 4.13-4.15 compare the experimental ΔP and the calculated ΔP at varying u_g, L_0, and total pressures, P. The accuracy of Eq. (4.3) for the H_2S-N_2 system in this study is demonstrated in Figure 4.16, where the maximum scatter (maximum deviation of model from experiment) of the data is found to be ±34 Pa at all measured values of pressure drop, demonstrated by the dashed lines.

The pressure drop over the course of two experiments is shown in Figure 4.17. The pressure drop over the fixed-bed increased over the course of the operating period, which is due to change in the structure of adsorbent particles. But the change of pressure drop over the course of adsorption process is only about 10 Pa less than the errors caused by Eq. (4.3). Thus Eq. (4.3) can be used to evaluate the pressure drop in the adsorption process.

4.6 Breakthrough behaviors for regenerated adsorbents

Breakthrough curves are determined by the global kinetics of the adsorption process. The characteristics of adsorbents have an important influence on the adsorption process. The regeneration methods chosen to regenerate the spent

Table 4.4 The measured and calculated pressure drop of the CG-4 bed

Run	u_g (m/s)	P (atm)	L_0 (cm)	u_0x10^3 (m/s)	ΔP[a] (pa)	ΔP[b] (pa)
1	0.09	50.0	24.5	1.70	27.56±0.01	22.3±0.2
2	0.14	50.0	24.5	1.80	67.53±0.03	57.3±0.2
3	0.18	50.0	24.5	3.40	99.92±0.05	108.2±0.3
4	0.26	50.0	24.5	5.20	132.21±0.07	165.6±0.3
11	0.26	40.0	24.5	6.50	70.29±0.04	86.9±0.4
12	0.26	10.0	24.5	26.0	39.28±0.02	13.3±0.1
4	0.26	50.0	24.5	5.20	132.21±0.07	165.6±0.3
10	0.26	50.0	17.0	5.20	101.99±0.05	114.9±0.5
9	0.26	50.0	11.5	5.20	90.96±0.05	77.7±0.3

a. Measured in the experiments at a H_2S inlet concentration of 3.00% v/v.

b. Calculated from the equation using Ψ_s=0.83, ε_{fb}=0.41.

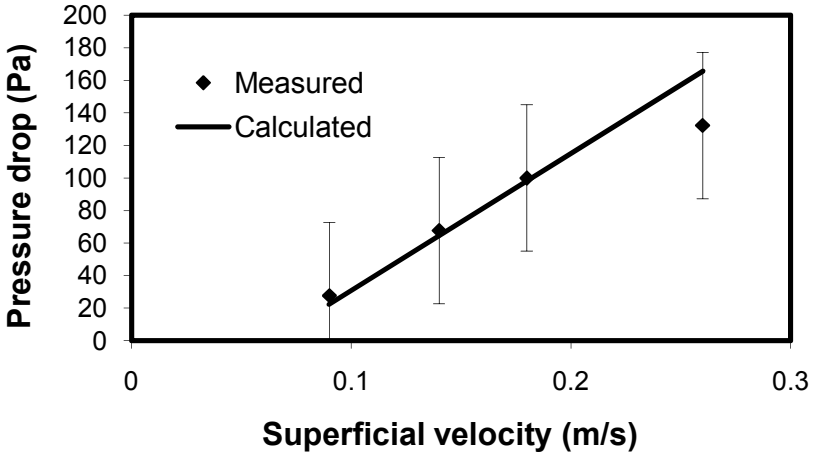

Figure 4.13 Comparison of the observed and the calculated pressure drop for different superficial velocities at P = 50 atm, $C_{A,in}$ = 3.00% v/v.

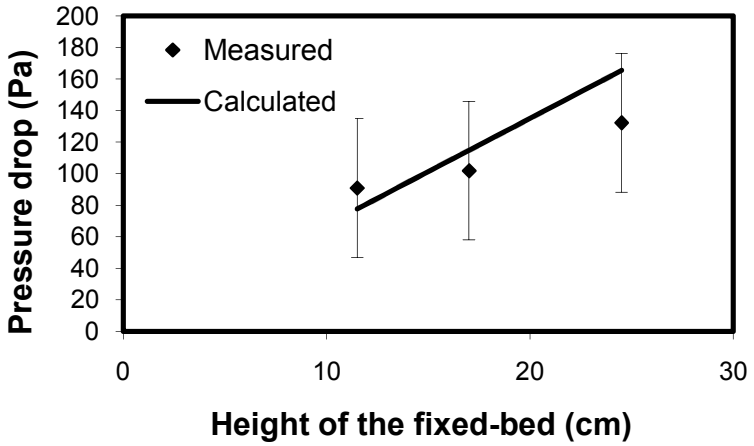

Figure 4.14 Comparison of the observed and the calculated pressure drop for different height of the fixed-bed at P = 50 atm, u_g = 0.26 m/s, $C_{A,in}$ = 3.00% v/v.

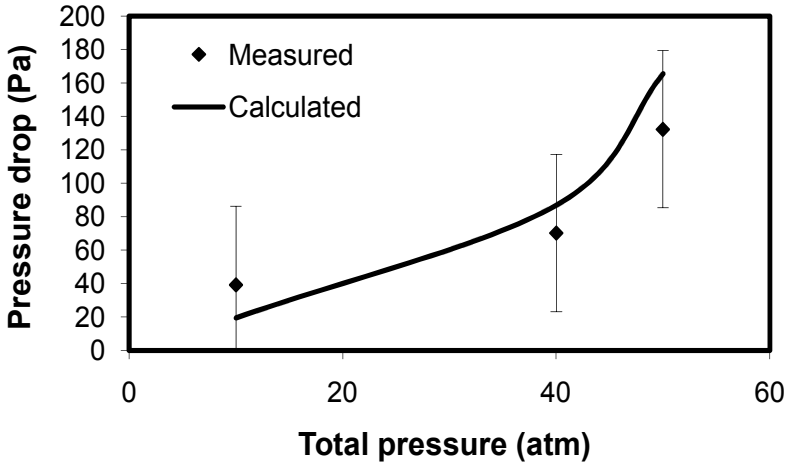

Figure 4.15 Comparison between the observed and the calculated pressure drop for different total pressures at at u_g = 0.26 m/s, L_0 = 24.5 cm $C_{A,in}$ = 3.00% v/v.

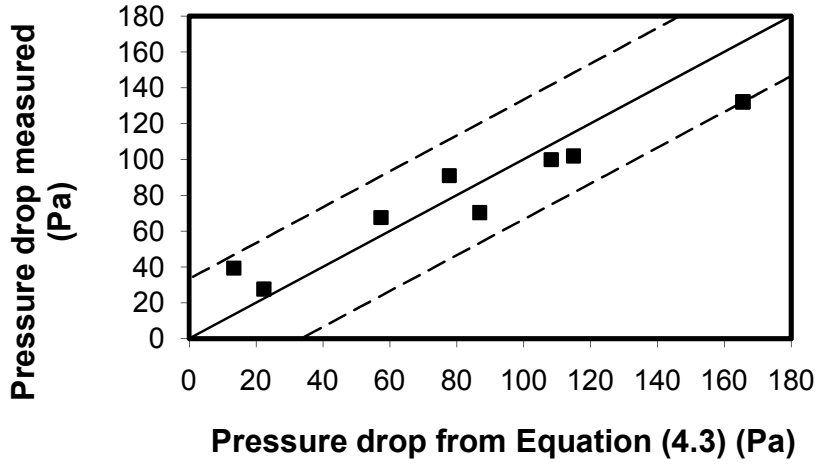

Figure 4.16 Parity plot showing scatter of pressure drop to the prediction of Eq. **(**4.3). Dashed lines show the maximum deviation.

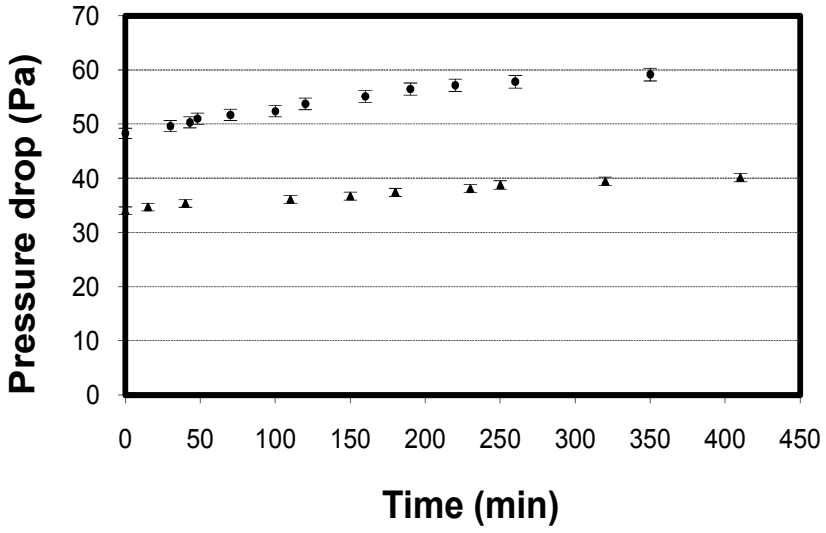

Figure 4.17 Pressure drop versus time for u_g = 0.26 m/s (●) at 30 atm with 0.50% v/v H_2S; (▲) at 15 atm with 1.00 %v/v H_2S.

adsorbent can alter the characteristics of the adsorbent, and therefore have an impact on the breakthrough curves. In this study, breakthrough curves were measured for adsorbents regenerated using air and using liquid ammonia.

When the spent adsorbent is exposed to air, Fe_2S_3 is oxidized to Fe_2O_3 and elemental sulfur and a part of the adsorbent activity is restored naturally. In the meantime, elemental sulfur deposition in the air-regenerated adsorbent causes a decrease in activity and sulfur loading when compared to the virgin adsorbent.

Ammonia leaching is considered a feasible treatment to remove elemental sulfur from the used adsorbents (Boudou *et al*., 2003; Wang *et al*., 2008). The air-regenerated adsorbent (regenerated by exposing to air for 24 h) was leached by using Wang's method (2008); that is, the air-regenerated adsorbent is leached continuously for 3 hours until the leachate was no longer coloured. The breakthrough curves for the virgin, air-regenerated, and ammonia-leached adsorbents are depicted in Figure 4.18. The sulfur loading for the air-regenerated adsorbent is about 3.5% w/w, only 16% of that of the virgin sample. The sulfur loading for the ammonia-leached adsorbent is 8% w/w, about one third of that of the virgin sample. The breakthrough curve for the air-regenerated adsorbent was distinctly wider and less steep than those for the virgin and ammonia-leached adsorbents. It can be concluded that the apparent reaction rate in the air-regenerated adsorbent is slower than the others. It is easy to understand that there is larger diffusion resistance in the solid layer due to the deposition of elemental sulfur. This is consistent with the findings of Wang *et al*. (2008). From Table 4.5, it is observed that only about 40% of sulfur in the spent adsorbent can be leached

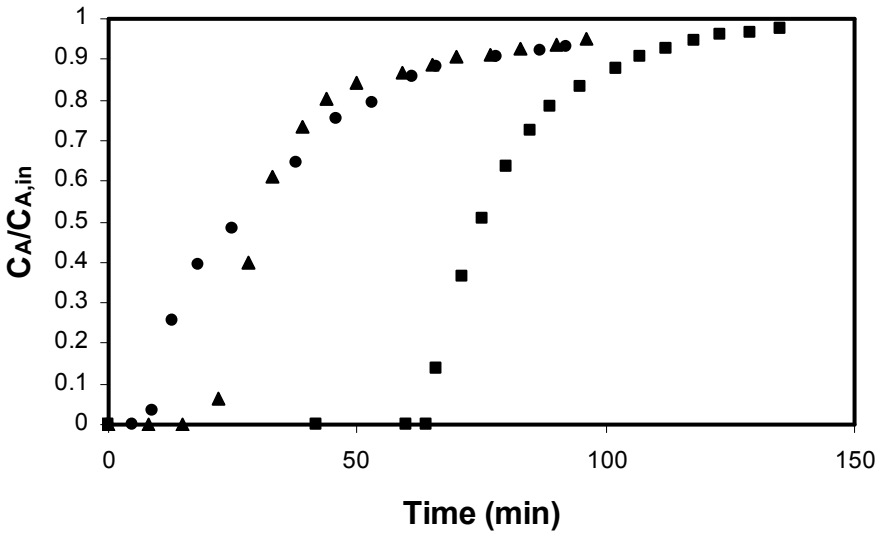

Figure 4.18 Breakthrough curves for ■ virginadsorbent, ▲ leached adsorbent, and ● air-regenerated adsorbent at 3.00% v/v, 1500 mL/min, 50 atm absolute.

Table 4.5 Results of ICP element analysis for virgin adsorbent, air-regenerated adsorbent and ammonia-leached adsorbent

Element	virgin sample % w/w	Spent sample % w/w	Leached sample % w/w	leachate % w/w
Al	0.042	0.034	0.035	0.0029
Ca	4.210	3.320	3.380	0.020
Fe	45.00	34.90	37.50	0.071
Mg	0.140	0.110	0.120	0.009
Mn	0.167	0.136	0.146	0.0011
P	0.002	0.002	0.002	0.0007
Na	0.05	0.05	0.04	0.022
Ti	0.421	0.332	0.355	0.0010
S	3.4	25.8	15.3	83.4

with ammonia. The leachate obtained by using Wang's ammonia leaching method (2008) consists mainly of elemental sulfur as shown in Table 4.5. It can be postulated that over half of the sulfur exists in the form of Fe_2S_3 as opposed to elemental sulfur. Sulfur in the form of Fe_2S_3 decomposes to FeS_2 and Fe_8S_9. Since Fe_8S_9 can not be oxidized, and the oxidization of FeS_2 to Fe_2O_3 is extremely slow (Crynes, 1977), this Fe_2S_3 remains bound to the adsorbate and is not removed during regeneration.

4.7 Regression analysis of the breakthrough behaviors

Since the fixed bed reactor is operated in an unsteady state, the transient of the reactor's outlet gas compositions depends on the operating conditions. In order to predict the transients of the outlet gas compositions, complex differential and energy balance equations based on the rate data for a single particle need to be solved. Several methods for solving these equations are discussed in Chapter 2. Due to lack of rate data for an iron oxide particle reaction with H_2S, a theoretical model can not be provided. A trial has been done to obtain the apparent kinetics (Appendix F), but the models can not describe the experimental data of the adsorption process in this study.

From a practical point of view, therefore, an empirical equation was developed from the experimental breakthrough curves by using the commercial software, Labfit. The curve fitting shows the following equation fits the experimental data:

$$\frac{C_A}{C_{A,in}} = 1 - A e^{-B t} \tag{4.5}$$

where C_A is outlet H_2S concentration % v/v, $C_{A,in}$ is inlet H_2S concentration % v/v, t starts at the breakthrough moment (s), and A and B are parameters to be determined by the operating conditions.

Figures 4.19 to 4.21 show the experimental data and the calculated breakthrough curves. It should be noted again that the starting point in the breakthrough curve, now, $t = 0$, is the time at which H_2S starts to breakthrough. The model parameters A and B were calculated by regression analysis and the results of the regression analyses for all runs are listed in Table 4.6. The value R^2 shows a good correlation between t and $\ln C_A$. Parameter A has no significant changes over all operating conditions and the average is 1.00±0.02. Physically, parameter A must be equal to 1 to make

$$\frac{C_A}{C_{A,in}} = 0 \text{ at } t = 0. \tag{4.6}$$

It is interesting to find that a linear correlation exists between mass flux of H_2S in the inlet gas and parameter B under all the operating conditions of $C_{A,in}$, u_g, and P:

$$B = 0.0026 \times \text{mass flux of } H_2S \quad (R^2 = 0.9927) \tag{4.7}$$

where mass flux of H_2S is in g/m^2-s.

The parameter B increases with increases in either the inlet gas H_2S concentration or the superficial velocity of feed gas stream. At the same concentration of H_2S and superficial velocity, the change in operating pressure does not change the mass flux of H_2S in inlet gas and the parameter B remains the same. Therefore the shape of breakthrough curves is the same as shown in Figure 4.3.

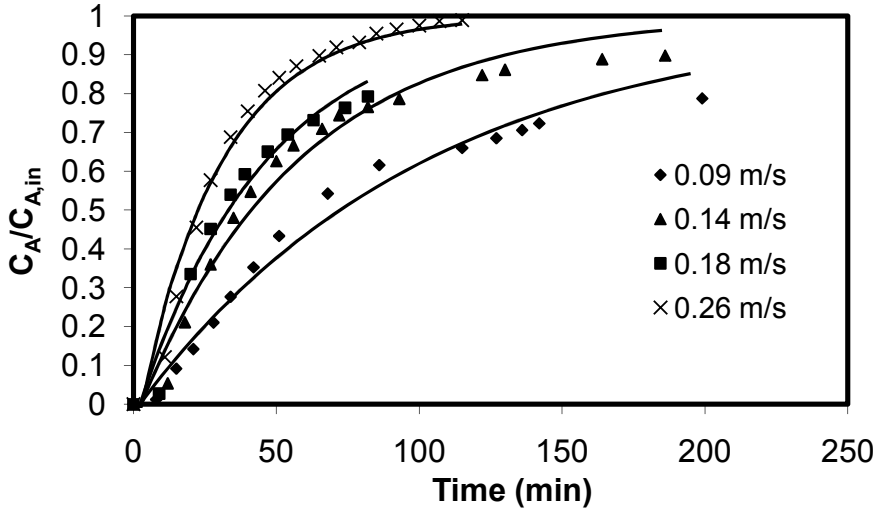

Figure 4.19 Comparison of the measured and predicted breakthrough curves for different superficial velocities at P = 50 atm, $C_{A,in}$ = 3.00% v/v. Solid lines represent the predicted values.

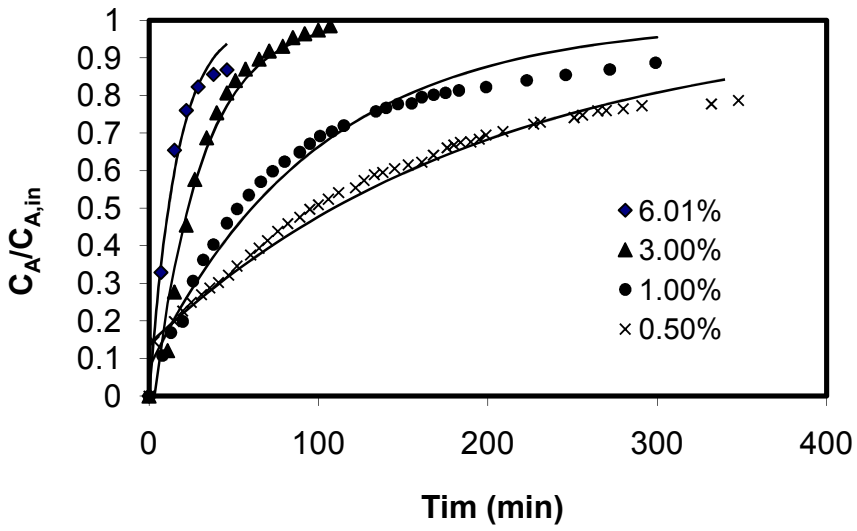

Figure 4.20 Comparison of the measured and predicted breakthrough curves for different H_2S concentrations at P = 50 atm, u_g = 0.26 m/s. Solid lines represent the predicted values.

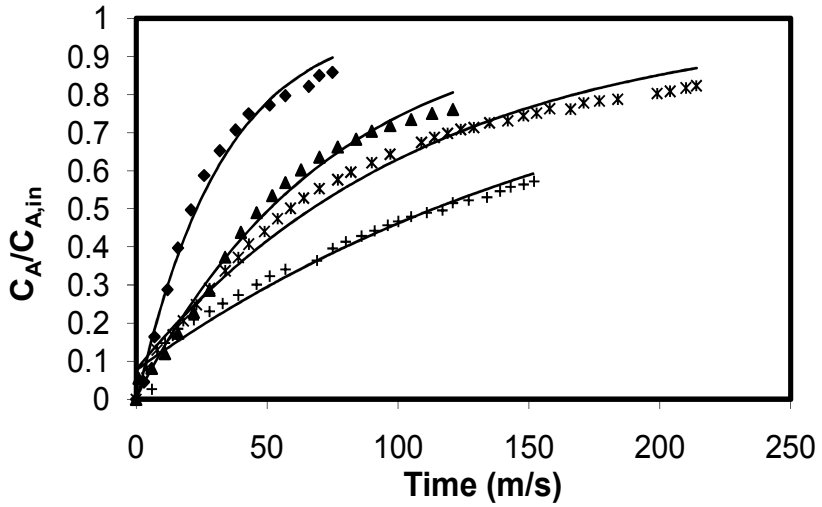

Figure 4.21 Comparison of the measured and predicted breakthrough curves for different pressures and different concentrations at u_g = 0.26 m/s (×: P = 5 atm, $C_{A,in}$ = 3.00% v/v; ▲: P = 10 atm, $C_{A,in}$ = 1.50% v/v; ■: P = 15 atm, $C_{A,in}$ = 1.00% v/v; ♦: P = 30 atm, $C_{A,in}$ = 0.50% v/v).

Table 4.6 Parameters *A* and *B* with the 95% confidence intervals for the empirical Eq. (4.5) at different conditions

Run	u_g (m/s)	$C_{A,in}$ (v/v)	P (atm)	A	B	R^2
1	0.09	0.0300	50.00	1.02±0.01	0.010±0.001	0.981
2	0.14	0.0300	50.00	1.05±0.02	0.018±0.001	0.976
3	0.18	0.0300	50.00	1.05±0.01	0.022±0.001	0.973
4	0.26	0.0300	50.00	1.10±0.02	0.034±0.002	0.979
5	0.26	0.0050	50.00	0.86±0.01	0.005±0.001	0.979
6	0.26	0.0100	50.00	0.92±0.02	0.010±0.001	0.976
7	0.26	0.0300	50.00	1.10±0.02	0.034±0.001	0.978
8	0.26	0.0601	50.00	0.99±0.01	0.060±0.001	0.985
9	0.26	0.0050	30.00	0.92±0.01	0.005±0.001	0.981
10	0.26	0.0100	15.00	0.92±0.01	0.009±0.002	0.984
11	0.26	0.0150	10.00	1.00±0.01	0.014±0.002	0.990
12	0.26	0.0300	5.00	1.01±0.02	0.030±0.001	0.991

The uncertaity of Eq (4.5) (for operating condition of P = 5 atm, u_g = 0.26 m/s, and $C_{A,in}$ = 3.00% v/v.) in terms of 95% confidence intervals is shown in Figure 4.22. Under other conditions Eq. (4.5) has similar confidence intervals.

In industrial practice, two vessels are arranged in lead/lag configuration as mentioned in Chapter 2. Eqs (4.5) and (4.7) can be used to determine the time needed for the adsorbent in one of two vessels to become saturated. Eq. (4.5) provides an easy tool for companies to predict the running period between media change-overs.

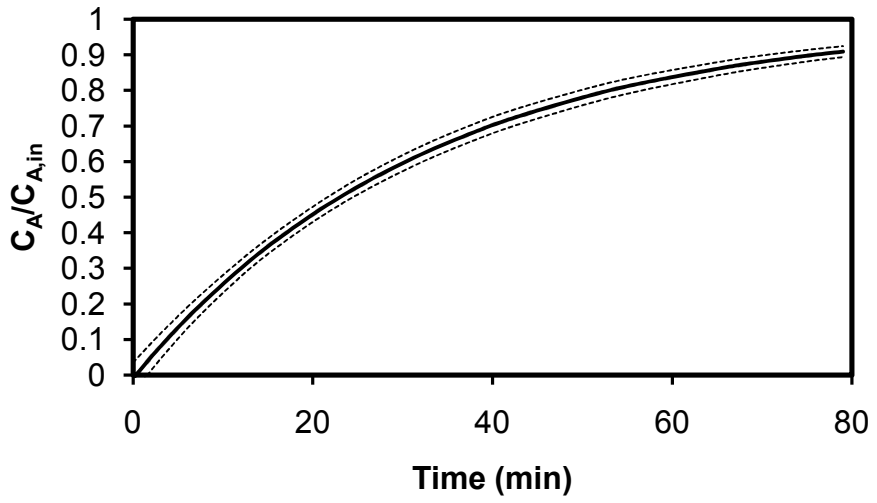

Figure 4.22 The uncertainty of Eq (4.5) with the 95% confidence intervals at P = 5 atm, u_g = 0.26 m/s, and $C_{A,in}$ = 3.00% v/v.

Chapter 5
Conclusions and Recommendations

5.1 Conclusions

The breakthrough curves for the CG-4 iron oxide adsorbent in the fixed-bed were measured and analyzed at different operating conditions. The parameters for the breakthrough curve, such as stoichiometric time (t_s) and length of unused bed (*LUB*) were calculated along with breakthrough points and sulfur loadings at superficial velocities of 0.09-0.26 m/s, H_2S inlet concentration of 0.50-6.01% v/v, pressure of 4-50 atm, and bed height of 11.5-24.5 cm.

Changing operating pressure within a range of 4-50 atm at constant H_2S concentration had no obvious impact on the shape of the breakthrough curve, the sulfur loading, or the length of unused bed (*LUB*).

The effect of changes in superficial velocity was more complex. The breakthrough curves appeared at later times and became wider as the superficial velocities (gas velocity) decreased. With an increase in the superficial velocity from 0.09 m/s to 0.25 m/s the length of unused bed proportionally increased and the utilization efficiency of the bed decreased. Thus, it was concluded that the sulfur loading lowers because of the decrease in retention time of the gas stream in the fixed-bed reactor.

Changes in the concentration of H_2S in the feed gas stream had an effect on the process from a kinetics point of view. Wider and flatter breakthrough curves

were obtained as the concentration of H_2S decreased. The utilization efficiency of the fixed-bed increased, as the H_2S inlet concentration decreased from 6.01 to 0.50% v/v.

Change in the height of the fixed-bed from 11.5 to 24.5 cm had no impact on the shape of the breakthrough curves, indicating that a fully-developed flow assumption is acceptable for this system under the range of operating conditions, leading to a constant transition zone within the fixed-bed reactor. However, the utilization efficiency of the fixed-bed and the sulfur loading increased with an increase in the height of the fixed-bed.

The sulfur loading for used adsorbent regenerated by exposing it to air is about 3.5% w/w, only 16% of the virgin sample's sulfur loading under the same operating conditions. The sulfur loading for used adsorbent regenerated by ammonia leaching is 8.0% w/w under similar conditions.

A simple empirical expression was proposed to predict the breakthrough curves and their evolution with time. The parameter *B* in the empirical expression has a linear correlation with the mass flux of H_2S in the feed gas stream. A good agreement between measured and predicted exit gas compositions versus time curves shows that this expression can be used for this process in a wide range of operating conditions.

In summary, the CG-4 adsorbent is effective for removal of H_2S in natural gas processing. Sulfur loading is mainly dependent on the residence time and mass flux of H_2S in the fixed-bed. The suggested residence time and mass flux of

H_2S are more than 3 seconds and less than 11.3 g/m^2-s respectively. The optimum values for practical use should be decided by considering economic factors.

5.2 Recommendations

The impact of the adsorption operating conditions on the breakthrough curves and the sulfur loading has been investigated. Further investigation needs to be done to observe how the structure of the adsorbent changes over the course of the adsorption process and how it causes the breakthrough curves and sulfur loadings change.

Although regression analysis was used to obtain the empirical correlation between exit gas H_2S concentration and time, it is believed that the correlation can give some directions to understanding the kinetics of this process. For instance, the parameter B is very close to the inlet H_2S concentration under the experimental conditions. Further study may disclose why this is so.

In order to further understand this adsorption process, the reaction kinetics for single grain needs to be studied. In addition, the effect of changing the operating temperatures on the breakthrough curve and sulfur loading can be investigated. This would help to develop a theoretical model.

In this study, the deep injection method for disposal of the spent adsorbent was initially suggested, but not investigated. Before approving of such an operation, the regulatory agencies need to review applications to maximize conservation of hydrocarbon resources, minimize environmental impacts, and ensure public safety. Detailed research needs to be carried out before such approval will be given.

References:

Adanez, J., A. Abad, F. Garcia-Labiano, L.F. de Diego, and P. Gayan, "H_2S Retention with Ca-Based Sorbents in a Pressurized Fixed–Bed Reactor: Application to Moving-Bed Design," Fuel, 84, 533-542 (2005).

Adanez, J., A. Abad, F. Garcia-Labiano, L.F. de Diego, and P. Gayan, "Direct Sulfidation of Half–Calcined Dolomite under Pressurized Conditions," Industrial and Engineering Chemistry Research, 43, 4132-4139 (2004).

Adanez, J., L.F. de Diego, F. Garcia-Labiano, and A. Abad, "Kinetics of H_2S Reaction with Calcined Calcium-Based Sorbents," Energy and Fuels, 12, 617-625 (1998).

Bachu, S., and W. D. Gunter, "Overview of Acid-Gas Injection Operations in Western Canada", Proceedings of 7th International Conference on Green House Gas Control Technologies (2005).

Bhatia, S. K., and D. D. Perlmutter, "A Random Pore Model for Fluid–Solid Reactions, I: Isothermal, Kinetic Control," AIChE Journal, 26, 379–386 (1980).

Bhatia, S.K., and D. D. Perlmutter, "A Random Pore Model for Fluid–Solid Reactions, II: Diffusion and Transport Effects," AIChE Journal, 20, 247–254 (1981).

Bhattacharya, A., and P. Purohit, "Predicting Reaction Rates for Non-Catalytic Fluid-Solid Reactions in Presence of Structural Changes in the Solid Phase," Chemical Engineering Journal, 102, 141-149 (2004).

Boudou, J.P., M. Chehimi, E. Broniek, T. Siemieniewsha and J. Bimer, "Adsorption of H_2S or SO_2 on an Activated Carbon Cloth Modified by Ammonia Treatment," Carbon, 41(10), 1999 (2003).

Clean Air Act, S.S. 1986-87-88, c. C-12.1, 1989.

Crynes, B. L., "Chemical Reactions as a Means of Separation: Sulfur Removal," Marcel Dekker, New York (1977), pp. 212-223.

Efthimidias, E.A., and S.V. Sotirchos, "Experimental Validation of a Mathematical Model for Fixed-Bed Desulfurization," AIChE Journal, 39(1), 99-110 (1993).

Fenouil, L. A., and S. Lynn, "Design of Entrained-Flow and Moving-, Packed-, and Fuidized-Bed Sorption Systems: Grain-Model Kinetics for Hot Coal-Gas Sulphurization with Limestone," Industrial and Engineering Chemistry Research, 35 (2), 1024-1043 (1996).

Fogler, H. S., "Elements of Chemical Engineering," 4th ed., Prentice Hall Professional, New Jersey (2006), pp. 880-886.

Froment, G. F., and K. B. Bischoff, "Chemical Reactor Analysis and Design," 2nd ed., John Wiley & Sons, New York (1990), pp.314-327.

Garcia-Labiano, F., "Effect of Pressure on the Sulfidation of Calcined Calcium-Based Sorbents," Energy & Fuels, 18, 761-769 (2004).

Gómez-Barea, A., and P. Ollero, "An Approximate for Solving Gas-Solid Non-Catalytic Reactions," Chemical Engineering Science, 61, 3725-3735 (2006).

Gottifredi, J. C., and E. E. Gonzo, "Approximate Expression for Predicting Concentration and Temperature Profiles inside a Catalyst Pellet," Chemical Engineering Science, 51, 835–837 (1996).

Gottifredi, J. C., and E.E. Gonzo, "Approximate Expression for the Effectiveness Factor Estimation and a Simple Numerical Method for Concentration Profile Calculation in Porous Catalyst," Chemical Engineering Journal, 109, 83–87 (2005).

Ilaria Rosso, " Zinc Oxide Sorbents for the Removal of Hydrogen Sulfide from Syngas," Industrial and Engineering Chemistry Research, 42, 1688-1697 (2003).

Jamshidi, E., and H. Ale-Ebrahim, "An Incremental Analytical Solution for Gas–Solid Reactions: Application to the Grain Model," Chemical Engineering Science, 51, 4253–4257 (1996).

Jamshidi, E., and H. Ale-Ebrahim, "A New Solution Technique of Moving Boundary Problems for Gas–Solid Reactions: Application to Half-Order Volume Reaction Model," Chemical Engineering Journal, 63, 79–83 (1996).

Jamshidi, E. and H. Ale-Ebrahim, "A Quantized Solution for the Nucleation Model in Gas–Solid Reactions," Chemical Engineering Journal, 68, 1–6 (1997).

Jamshidi, E., and H. Ale-Ebrahim, "A New Solution Technique for Gas–Solid Reactions with Structural Changes," Chemical Engineering Science, 54, 859–864 (1999).

Kohl, A., and R. Neilson, "Gas Purification," Golf Publishing Company, Houston, Texal (1997), pp. 253-268.

Lee, D. K., "An Apparent Kinetic Model for the Carbonation of Calcium Oxide by Carbon Dioxide," Chemical Engineering Journal, 100, 71-77 (2004).

McGuckin, R.L., "Pressure Drop through Raw Food Waste Compost Containing Synthetic Bulking Agents," Journal of Agricultural Engineering Research, 72, 375-84 (1999).

Miura, K., "Simultaneous Removal of COS and H_2S from Coke and Oven Gas at Low Temperature by Use of an Iron Oxide," Industrial and Engineering Chemistry Research, 31, 415-419 (1992).

Park, H. C., S. Kimura, and Y. Sakai, "An Unsteady State Analysis of Packed Bed Reactors for Gas-Solid Reactions," Journal of Chemical Engineering of Japan, 17 (3), 269-274 (1984).

Patnaik, P., "A Comprehensive Guide to the Hazardous Properties of Chemical Substances," 2nd ed., John Wiley, New York (1999), pp. 505-536.

Poling, B.E., J. M. Prausnitz, J. P. O'Conneil, "The Properties of Gases and Liquids," 5th ed., Mcgraw –Hill, New York (2001), pp. 454-470.

Qiu, K., and O. Lindqvist, "Direct Sulfation of Limestone at Elevated Pressures," Chemical Engineering Science, 55, 3091-3100 (2000).

Ramachandran, P. A., "Analytical Prediction of Conversion-Time Behavior of Gas–Solid Noncatalytic Reaction," Chemical Engineering Science, 38, 1385–1390 (1983).

Sardesai, P., "Exploring the Gas Anaerobic Bioremoval of H_2S for Coal Gasification Fuel Cell Feed Streams," Fuel Processing Technology, 87, 319-324 (2006).

Sotirchos, S. V., and H.-C. Yu, "Overlapping Grain Models for Gas-Solid Reactions with Solid Product," Industrial and Engineering Chemistry Research, 27, 836-845 (1988).

Speight, J. G., "Fuel Science and Technology Handbook," Marcel Dekker, New York (1990), pp. 137-149.

Sublette, K. L., and N. D. Sylvester, "Oxidation of Hydrogen Sulfide: Desulfurization of Natural Gas," Biotechnology and Bioengineering, 29, 595-600 (1987).

Turton, R., "Evaluation of Zinc Oxide Sorbents in a Pilot-Scale Transport Reactor: Sulfidation Kinetics and Reactor Modeling," Industrial and Engineering Chemistry Research, 43, 1235-1243 (2004).

Wang, H., D. Fang, and K.T. Chuang, "A Sulfur Removal and Disposal Process through H_2S Adsorption and Regeneration: Ammonia Leaching Regeneration," Process Safety and Environment Protection, 8, 296-302 (2008).

Wang, L. K., "Advanced Air and Noise Pollution Control," Humana Press, New York (2004), pp. 367-420.

Welty, J. R., "Fundamentals of Momentum, Heat, and Mass Transfer," 4^{th} ed., John Wiley & Sons, New York (2001), pp.263-274.

Xu, J., and U. Hoffmann, "Application of Integral Transformation and Orthogonal Collocation in Gas–Solid Non-Catalytic Reaction with Varying Diffusivity, Temperature and Bulk Gas Concentration," Chemical Engineering Science, 44, 1431–1440 (1989).

Xue, M., R. Chitrakar, K. Sakane, and K. Ooi, "Screening of Adsorbents for Removal of H_2S at Room Temperature," Green Chemistry, 5, 529-534 (2003).

Appendix A: Calibration table and curve for TCD

A1. Calibration table for TCD

RT (min)	Compound	Amount (ppm)	Area
2.4	H_2S	858	16.2
		1001	21.7
		1040	22.1
		2003	46.1
		3756	92.2
		7513	189.1
		12020	316.7
		20030	536.2
		30050	801.3
		60100	1820.0

A2. Calibration curve for TCD

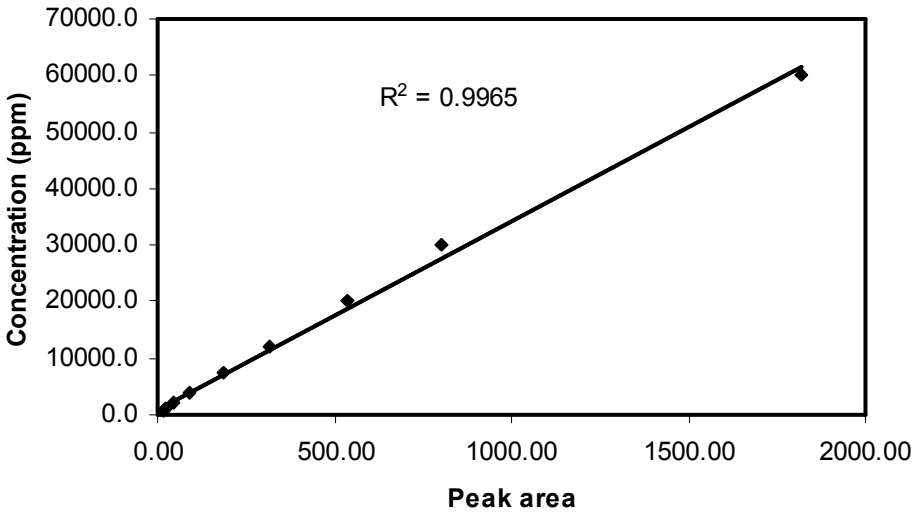

Calibration equation expressed in terms of the 95 % confidence intervals for the slope and intercept is:

Concentration (ppm) = (33.2 ± 0.4)*peak area + (1100 ± 320)

.

Appendix B: Calibration table and curve for FPD

B1. Calibration table for FPD

RT (min)	Compound	Amount (ppm)	Area
2.41	H_2S	50	3558
		80	10193
		115	23287
		173	60437
		260	166340
		347	247000
		520	303570
		858	616570
		1040	696160

B2. Calibration curve for FPD

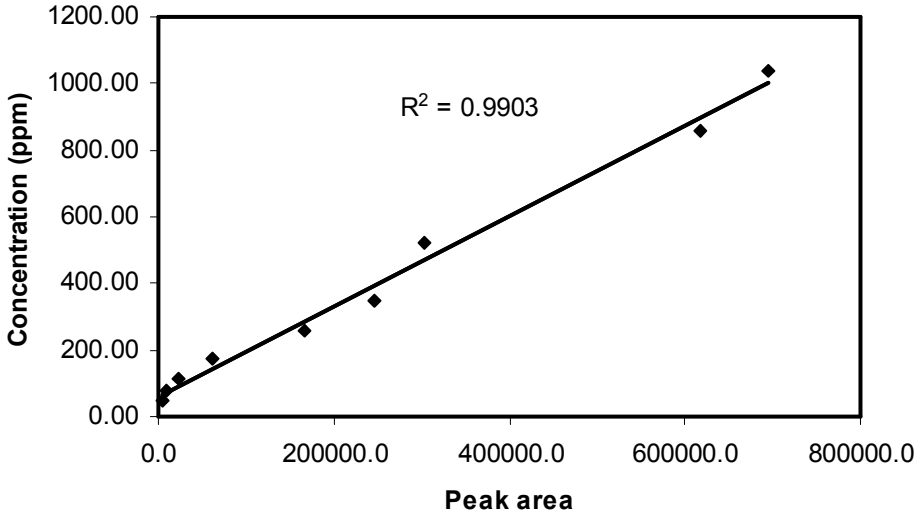

Calibration equation expressed in terms of the 95 % confidence intervals for the slope and intercept is:

Concentration (ppm) = (0.00134 ± 0.00006)*peak area + (68±20)

Appendix C: Calibration curves for mass flow controllers

C1. Calibration curve for mass flow controller 5850S (10 L/min)

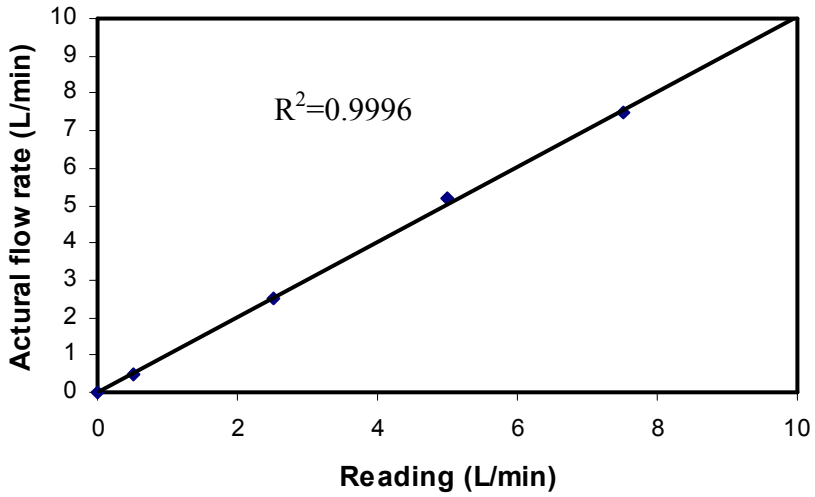

Calibration equation expressed in terms of the 95 % confidence intervals for the slope and intercept is:

Flow rate (L/min) = (1.004 ± 0.002)*peak area - (0.01±0.01)

C2. Calibration curve for mass flow controller 5850S (1 L/min)

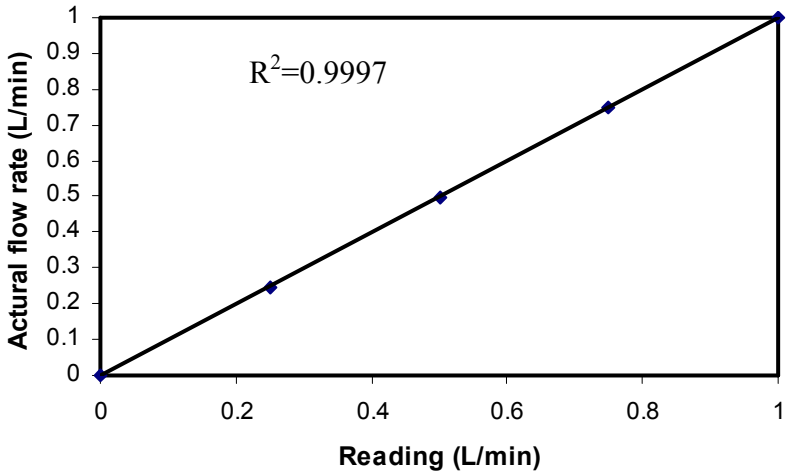

Calibration equation expressed in terms of the 95 % confidence intervals for the slope and intercept is:

Flow rate (L/min) = (1.005 ± 0.002)*peak area - (0.004±0.001)

Appendix D:

Conversion of the mass flow controller for a different gas than for which it is calibrated

D1. Gas factor table

Gas name	N_2	H_2S	CH_4
Gas factor	1.000	0.850	0.763

D2. For a pure gas:

$$\text{Actual gas flow rate} = \text{output reading} \times \frac{\text{factor of the new gas}}{\text{factor of the calibrated gas}(N_2)}$$

D3. For mix gases:

1. Calculate gas factor for mix gases

$$\text{Factor for mixture} = \frac{100}{\frac{P1}{\text{factor of gas 1}} + \frac{P2}{\text{factor of gas 2}} + \times\times + \frac{Pn}{\text{factor of gas n}}}$$

Where P1 percentage (%) of gas 1 (by volume)
P2 percentage (%) of gas 2 (by volume)
Pn percentage (%) of gas n (by volume)

2. Calculate the actual flow rate

$$\text{Actual gas flow rate} = \text{output reading} \times \frac{\text{factor of the mixture gas}}{\text{factor of the calibrated gas}(N_2)}$$

Appendix E: Raw data of breakthrough experiment at superficial velocity 0.26 m/s, pressure 50 atm

Table E1 Raw data of breakthrough experiment at H_2S concentration 0.50 % v/v

Time (min)	$C_A/C_{A,in}$ (measured)	$C_A/C_{A,in}$ (calculated)
0	0	0
3	0.146	0.151
15	0.198	0.202
20	0.227	0.222
25	0.250	0.242
31	0.270	0.265
36	0.288	0.284
41	0.302	0.302
47	0.322	0.323
52	0.346	0.340
60	0.376	0.367
65	0.394	0.383
70	0.414	0.399
76	0.439	0.417
82	0.459	0.435
89	0.476	0.455
95	0.497	0.471
100	0.510	0.485
106	0.524	0.500
112	0.542	0.515
122	0.555	0.540
127	0.574	0.551
133	0.589	0.565
138	0.596	0.576
145	0.606	0.591

153	0.616	0.608
161	0.623	0.623
168	0.642	0.637
176	0.661	0.651
180	0.669	0.658
184	0.675	0.665
190	0.677	0.675
195	0.684	0.684
199	0.695	0.690
209	0.705	0.706
227	0.724	0.732
231	0.729	0.737
251	0.742	0.763
256	0.748	0.759
265	0.759	0.779
270	0.760	0.785
280	0.765	0.796
291	0.773	0.807
332	0.778	0.844
348	0.787	0.856
360	0.811	0.860

Table E2 Raw data of breakthrough experiment at H_2S concentration 1.00 % v/v

Time (min)	$C_A/C_{A,in}$ (measured)	$C_A/C_{A,in}$ (calculated)
0	0	0
8	0.108	0.148
13	0.169	0.189
20	0.199	0.245
26	0.306	0.289
32	0.363	0.331
38	0.403	0.371
46	0.460	0.419
52	0.498	0.453
59	0.535	0.491
66	0.570	0.525
73	0.599	0.558
80	0.624	0.624
89	0.649	0.646
95	0.672	0.667
101	0.693	0.689
108	0.704	0.710
115	0.720	0.760
134	0.758	0.775
140	0.767	0.790
147	0.778	0.806
155	0.779	0.818
161	0.796	0.830
168	0.803	0.842
175	0.808	0.854
183	0.814	0.876

199	0.823	0.902
223	0.841	0.923
246	0.855	0.940
272	0.870	0.950

Table E3 Raw data of breakthrough experiment at H_2S concentration 3.00 % v/v

Time (min)	$C_A/C_{A,in}$ (measured)	$C_A/C_{A,in}$ (calculated)
0	0	0
11	0.121	0.240
15	0.277	0.340
22	0.455	0.480
27	0.577	0.570
34	0.688	0.660
40	0.754	0.730
46	0.807	0.775
51	0.840	0.812
57	0.870	0.846
65	0.897	0.883
71	0.919	0.905
79	0.931	0.928
85	0.954	0.941
92	0.964	0.954
100	0.974	0.965
107	0.986	0.973

Table E4 Raw data of breakthrough experiment at H_2S concentration 6.01 % v/v

time (min)	$C_A/C_{A,in}$ (measured)	$C_A/C_{A,in}$ (calculated)
0	0	0
7	0.329	0.348
15	0.654	0.598
22	0.760	0.737
29	0.823	0.827
38	0.856	0.899
46	0.868	0.930

Appendix F:

Trial calculations using the unreacted shrinking core model and the grain model

According to Eq. (2.1), the reaction rate for H_2S is three times the Fe_2O_3 consumption rate, which may be written as:

$$\frac{\partial X}{\partial t} = \frac{1}{3 C_{B0}} k \, C_A{}^n F(X) \tag{A.1}$$

$$\frac{3C_{B0}}{F(X)} \frac{\partial X}{\partial t} = k \, C_A{}^n \tag{A.2}$$

At the bed exit, the above expression can be changed as follows:

$$\frac{3C_{B0}}{F(X)} \frac{dX}{dt} = k \, C_A{}^n \tag{A.3}$$

$$\ln\left(\frac{3C_{B0}}{F(X)} \frac{dX}{dt} \right) = \ln k + n \ln C_A \tag{A.4}$$

$$\text{Let } Y = \ln\left(\frac{3C_{B0}}{F(X)} \frac{dX}{dt} \right) = \ln k + n \ln C_A \tag{A.5}$$

Using Eqs (2.66), (2.67), and (2.90), the data $C_A / C_{A,in}$ at the outlet of the fixed bed at time t can be transferred to $F(X)$ at time t. The apparent kinetic reaction rate constant and reaction order should be determined by fitting the data of conversion profiles to Eq. (A.4) using Excel.

If these models can correctly describe the adsorption reaction, Y and $\ln C_A$ would be in linear relationship. Take the data of breakthrough experiment at H_2S concentration 1.00 % v/v (Table E2) for example, the unreacted shrinking core model were used to fit the data. The results are shown in Figure F.1. It is indicated

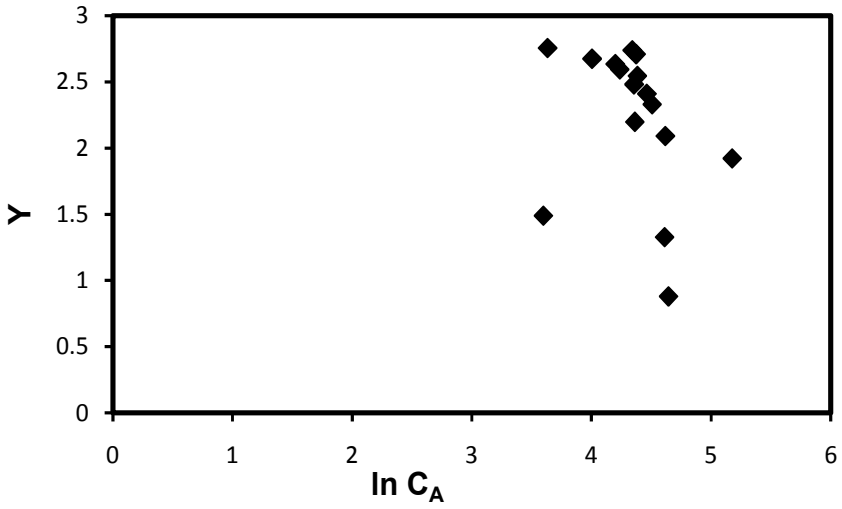

Figure F1 Plot of Y versus lnC_A

that this model can not describe the adsorption process. In this thesis, therefore, regression analysis was used to fit the data of conversion profiles over software Labfit.

Appendix G:

Praxair Material Safety Data Sheet (MSDS)

for hydrogen sulfide/inert gas mixture

Praxair Material Safety Data Sheet

1. Chemical Product and Company Identification

Product Name:	Hydrogen sulphide/inert gas mixture	**Trade Name:**	Hydrogen sulphide/inert gas mixture
Product Use:	Not available.		
Chemical Name:	Not applicable.	**Synonym:**	Not applicable.
Chemical Formula:	Not applicable.	**Chemical Family:**	Not applicable.
Telephone:	**Emergencies:** * 1-800-363-0042	**Supplier /Manufacture:**	Praxair Canada Inc. 1 City Centre Drive Suite 1200 Mississauga, ON L5B 1M2
		Phone:	905-803-1600
		Fax:	905-803-1682

**Call emergency numbers 24 hours a day only for spills, leaks, fire, exposure, or accidents involving this product. For routine information, contact your supplier or Praxair sales representative.*

2. Composition and Information on Ingredients

INGREDIENTS	% (VOL)	CAS NUMBER	LD_{50} (Species & Routes)	LC_{50} (Rat, 4 hrs.)	TLV-TWA (ACGIH)
Hydrogen sulphide AND CONTAINS ONE OR MORE OF THE FOLLOWING GASES:	0.0001-0.99	7783-06-4	Not applic.	356 ppm	10 ppm
Argon	Balance	7440-37-1	Not applic.	Not available.	Simple asphyxiant.
Helium	Balance	7440-59-7	Not applic.	Not available.	Simple asphyxiant.
Krypton	Balance	7439-90-9	Not applic.	Not available.	Simple asphyxiant.
Neon	Balance	7440-01-1	Not applic.	Not available.	Simple asphyxiant.
Nitrogen	Balance	7727-37-9	Not applic.	Not available.	Simple asphyxiant.
Xenon	Balance	7440-63-3`	Not applic.	Not available.	Simple asphyxiant.

3. Hazards Identification

Emergency Overview

CAUTION! High-pressure gas. Can cause rapid suffocation. May cause dizziness and drowsiness. Self-contained breathing apparatus may be required by rescue workers.

ROUTES OF EXPOSURE: Inhalation.

THRESHOLD LIMIT VALUE: TLV-TWA Data from 2007 Guide to Occupational Exposure Values (ACGIH). TLV-TWAs should be used as a guide in the control of health hazards and not as fine lines between safe and dangerous concentrations.

EFFECTS OF A SINGLE (ACUTE) OVEREXPOSURE:

INHALATION:	Asphyxiant. Moderate concentrations may cause headaches, drowsiness, dizziness, excitation, excess salivation, vomiting, and unconciousness. This mixture contains traces of hydrogen sulphide wihich may causesome irritation of the respiratory tract and damage the central nervous system if inhaled in large quantities.Lack of oxygen can kill.
SKIN CONTACT:	No evidence of adverse effects from available information.
SKIN ABSORPTION:	No evidence of adverse effects from available information.
SWALLOWING:	Unlikely route of exposure. This product is a gas at normal temperature and pressure.
EYE CONTACT:	No evidence of adverse effects from available information.

EFFECTS OF REPEATED (CHRONIC) OVEREXPOSURE:
No evidence of adverse effects from available information.

OTHER EFFECTS OF OVEREXPOSURE:
None known. This product is an asphyxiant. Lack of oxygen can cause death.

MEDICAL CONDITIONS AGGRAVATED BY OVEREXPOSURE:
Repeated or prolonged exposure is not known to aggravate medical condition.

SIGNIFICANT LABORATORY DATA WITH POSSIBLE RELEVANCE TO HUMAN HEALTH HAZARD EVALUATION:
Not available - mixture not tested.

CARCINOGENICITY:
Not listed as carcinogen by OSHA, NTP or IARC.

4. First Aid Measures

INHALATION:
If inhaled, remove to fresh air. If not breathing, give artificial respiration. If breathing is difficult, give oxygen. Get medical attention.

SKIN CONTACT:
Wash contaminated skin with soap and water.

SWALLOWING:
This product is a gas at normal temperature and pressure.

EYE CONTACT:
Flush with water.

NOTES TO PHYSICIAN:
There is no specific antidote. Treatment of over-exposure should be directed at the control of symptoms and the clinical condition.

5. Fire Fighting Measures

FLAMMABLE :	No.	**IF YES, UNDER WHAT CONDITIONS?**	Not applicable.
FLASH POINT (test method)	Not applicable.	**AUTOIGNITION TEMPERATURE**	Not applicable.

FLAMMABLE LIMITS IN AIR, % by volume:	**LOWER:**	Not applicable.	**UPPER:**	Not applicable.

EXTINGUISHING MEDIA:

This mixture cannot catch fire. Use media appropriate for surrounding fire.

SPECIAL FIRE FIGHTING PROCEDURES:

CAUTION! **High-pressure gas.** Asphxiant. Effects are due to lack of oxygen. Evacuate all personnel from danger area. Immediately deluge cylinders with water from maximum distance until cool; then move them away from fire area if without risk. Self-contained breathing apparatus may be required by rescue workers

UNUSUAL FIRE AND EXPLOSION HAZARD:

Nonflammable material. This material cannot catch fire. Container may rupture due to heat of fire. No part of a container should be subjected to temperature higher than 52 C. Most containers are provided with a pressure relief device designed to vent contents when they are exposed to elevated temperature. Toxic fumes may be produced when heated.

HAZARDOUS COMBUSTION PRODUCTS:

Not applicable.

SENSITIVITY TO IMPACT:

Avoid impact against container.

SENSITIVITY TO STATIC DISCHARGE:

Not applicable.

6. Accidental Release Measures

STEPS TO BE TAKEN IF MATERIAL IS RELEASED OR SPILLED:

CAUTION! **High-pressure gas.** Evacuate all personnel from danger area. Use self-contained breathing apparatus where needed. Shut off flow if you can do so without risk. Ventilate area or move cylinder to a well-ventilated area. Test for sufficient oxygen, especially in confined spaces, before allowing reentry.

WASTE DISPOSAL METHOD:

Prevent waste from contaminating the surrounding environment. Keep personnel away. Discard any product, residue, disposable container, or liner in an environmentally acceptable manner, in full compliance with federal, provincial, and local regulations. If necessary, call your local supplier for assistance.

7. Handling and Storage

PRECAUTIONS TO BE TAKEN IN STORAGE:

Store and use with adequate ventilation. Separate flammable cylinders from oxygen, chlorine, and other oxidizers by at least 6 m or use a barricade of non-combustible material. This barricade should be at least 1.5 m high and have a fire resistance rating of at least ½ hour. Firmly secure cylinders upright to keep them from falling or being knocked over. Screw valve protection cap firmly in place by hand. Post "No Smoking or Open Flames" signs in storage and use areas. There must be no sources of ignition. All electrical equipment in storage areas must be explosion-proof. Storage areas must meet national electric codes for Class 1 hazardous areas. Store only where temperature will not exceed 52 C. Store full and empty cylinders separately. Use a first-in, first-out inventory system to prevent storing full cylinders for long periods.

PRECAUTIONS TO BE TAKEN IN HANDLING:

Protect cylinders from damage. Use a suitable hand truck to move cylinders; do not drag, roll, slide, or drop. Never attempt to lift a cylinder by its cap; the cap is intended solely to protect the valve. Never insert an object (e.g., wrench, screwdriver, pry bar) into cap openings; doing so may damage the valve and cause a leak. Use an adjustable strap wrench to remove over-tight or rusted caps. Open valve slowly. If valve is hard to open, discontinue use and contact your supplier. For other precautions, see section 16.

For additional information on storage and handling, refer to Compressed Gas Association (CGA) pamphlet P-1, *Safe*

Handling of Compressed Gases in Containers, available from the CGA. Refer to section 16 for the address and phone number along with a list of other available publications.

OTHER HAZARDOUS CONDITIONS OF HANDLING, STORAGE, AND USE:

High pressure gas. Use piping and equipment adequately designed to withstand pressures to be encountered. ***Gas can cause rapid suffocation due to oxygen deficiency.*** Store and use with adequate ventilation. Close valve after each use; keep closed even when empty. ***Prevent reverse flow.*** Reverse flow into cylinder may cause rupture. Use a check valve or other protective device in any line or piping from the cylinder. ***When returning cylinder to supplier,*** be sure valve is closed, then install valve outlet plug tightly. ***Never work on pressurized system.*** If there is a leak, close the cylinder valve. Vent the system down in a safe and environmentally sound manner in compliance with all federal, provincial, and local laws; then repair the leak. ***Never place a compressed gas cylinder where it may become part of an electrical circuit.***

8. Exposure Controls/Personal Protection

VENTILATION/ENGINEERING CONTROLS:

LOCAL EXHAUST:	Preferred.
MECHANICAL (general):	Acceptable.
SPECIAL:	None.
OTHER:	Not applicable.

PERSONAL PROTECTION:

RESPIRATORY PROTECTION:	Select in accordance with provincial regulations, local bylaws or guidelines. Selection should also be based on the current CSA standard Z94.4, "Selection, Care and Use of Respirators". Respirators should also be approved by NIOSH and MSHA.
SKIN PROTECTION:	Wear work gloves when handling cylinders.
EYE PROTECTION:	Wear safety glasses when handling cylinders. Select in accordance with the current CSA standard Z94.3, "Industrial Eye and Face Protection", and any provincial regulations, local bylaws or guidelines.
OTHER PROTECTIVE EQUIPMENT:	Metatarsal shoes for cylinder handling. Protective clothing where needed. Cuffless trousers should be worn outside the shoes. Select in accordance with the current CSA standard Z195, "Protective Foot Wear", and any provincial regulations, local bylaws or guidelines.

9. Physical and Chemical Properties

PHYSICAL STATE:	Gas.	**FREEZING POINT:**	Not available - mixture not tested.	**pH:**	Not available - mixture not tested.
BOILING POINT	Not available - mixture not tested.	**VAPOUR PRESSURE**	Gas.	**MOLECULAR WEIGHT:**	Not applicable.
SPECIFIC GRAVITY: LIQUID (Water = 1)	Not applicable.	**SOLUBILITY IN WATER,**	Not available - mixture not tested.		
SPECIFIC GRAVITY: VAPOUR (air = 1)	Not available - mixture not tested.	**EVAPORATION RATE** (Butyl Acetate=1):	Not available.	**COEFFICIENT OF WATER/OIL DISTRIBUTION:**	Not applicable.

VAPOUR DENSITY:	Not available - mixture not tested.	**% VOLATILES BY VOLUME:**	Not available.	**ODOUR THRESHOLD:**	Not available.
APPEARANCE & ODOUR:	Colourless.	Rotten eggs.			

10. Stability and Reactivity

STABILITY:	The product is stable.
CONDITIONS OF CHEMICAL INSTABILITY:	Not available.
INCOMPATIBILITY (materials to avoid):	Not available - mixture not tested.
HAZARDOUS DECOMPOSITION PRODUCTS:	Not available - mixture not tested.
HAZARDOUS POLYMERIZATION:	Not available.
CONDITIONS OF REACTIVITY:	None currently known.

11. Toxicological Information

See section 3.

12. Ecological Information

No adverse ecological effects expected. This product does not contain any Class I or Class II ozone-depleting chemicals. The components of this mixture are not listed as marine pollutants by TDG Regulations.

13. Disposal Considerations

WASTE DISPOSAL METHOD: Do not attempt to dispose of residual or unused quantities. Return cylinder to supplier.

14. Transport Information

TDG/IMO SHIPPING NAME: Compressed gas, n.o.s.

HAZARD CLASS:	CLASS 2.2: Non-flammable and non-poisonous gas.	**IDENTIFICATION #:**	UN1956
PRODUCT RQ:	Any accidental release in a quantity that could pose a danger to public safety or any sustained release of 10 minutes or more		

SHIPPING LABEL(s): Non-flammable, non-poisonous gas

PLACARD (when required): Non-flammable, non-poisonous gas

SPECIAL SHIPPING INFORMATION:

Cylinders should be transported in a secure position, in a well-ventilated vehicle. Cylinders transported in an enclosed, nonventilated compartment of vehicle can present serious safety hazards.

15. Regulatory Information

The following selected regulatory requirements may apply to this product. Not all such requirements are identified. Users of this product are solely responsible for compliance with all applicable federal, provincial, and local regulations.

DSL (Canada) This product is on the DSL list

WHMIS (Canada) CLASS A: Compressed gas.

International Regulations

EINECS Not available.

DSCL (EEC) R20- Harmful by inhalation.

International Lists No products were found.

16. Other Information

MIXTURES:

When two or more gases, or liquefied gases are mixed, their hazardous properties may combine to create additional, unexpected hazards. Obtain and evaluate the safety information for each component before you produce the mixture. Consult an Industrial Hygienist, or other trained person when you make your safety evaluation of the end product. Remember, gases and liquids have properties which can cause serious injury or death.

HAZARD RATING SYSTEM:

HMIS RATINGS:

HEALTH	0
FLAMMABILITY	0
PHYSICAL HAZARD	2

STANDARD VALVE CONNECTIONS FOR U.S. AND CANADA:

THREADED:	CGA-330
PIN-INDEXED YOKE:	Not available.
ULTRA-HIGH-INTEGRITY CONNECTION:	Not available.

Use the proper CGA connections. **DO NOT USE ADAPTERS.** Additional limited-standard connections may apply. See CGA pamphlets V-1 and V-7 listed below.

Ask your supplier about free Praxair safety literature as referred to in this MSDS and on the label for this product. Further information about this product can be found in the following pamphlets published by the Compressed Gas Association, Inc. (CGA), 4221 Walney Road, 5th Floor, Chantilly, VA 20151-2923, Telephone (703) 788-2700, Fax (703) 961-1831, website: www.cganet.com.

AV-1	Safe Handling and Storage of Compressed Gas
P-1	Safe Handling of Compressed Gases in Containers
P-14	Accident Prevention in Oxygen-Rich, Oxygen-Deficient Atmosphere
SB-2	Oxygen-Deficient Atmospheres
V-1	Compressed Gas Cylinder Valve Inlet and Outlet Connections
V-7	Standard Method of Determining Cylinder Valve Outlet Connections for Industrial Gas Mixtures
---	Handbook of Compressed Gases, Fourth Edition

For more indepth information for each component, refer to the pure product MSDS.

The information contained in this MSDS is generated from technical sources using the Chemmate Mixture

MSDS system and the pure-product MSDS for each component. These mixtures are not tested as a whole for chemical, physical, or health effects.

PREPARATION INFORMATION:

DATE: **10/15/2007**
DEPARTMENT: **Safety and Environmental Services**
TELEPHONE: **905-803-1600**

The opinions expressed herein are those of qualified experts within Praxair Canada Inc. We believe that the information contained herein is current as of the date of this Material Safety Data Sheet. Since the use of this information and the conditions of use of the product are not within the control of Praxair Canada Inc., it is the user's obligation to determine the conditions of safe use of the product.

Praxair Canada Inc. requests the users of this product to study this Material Data Sheet (MSDS) and become aware of product hazards and safety information. To promote safe use of this product, a user should (1) notify its employees, agents and contractors of the information on this MSDS and any product hazards and safety nformation, (2) furnish this same information to each of its customers for the product, and (3) request such customers to notify their employees and customers for the product of the same product hazards and safety information.

Praxair Canada Inc.
1 City Centre Drive
Suite 1200
Mississauga, ON L5B 1M2